The perioperative occurrence of hypoxia and the balance between oxygen supply and demand in aortic arch surgery patients

A master's thesis for the degree of Technical Medicine

By Koen van der Veen

26 April 2024, Nijmegen

UNIVERSITY OF TWENTE.

Radboudumc

Abstract

Introduction The mismatch between the supply and demand of oxygen in the brain is an important pathway that can lead to cerebral ischemia, resulting in postoperative neurological dysfunction. Perioperative multimodal monitoring could provide insight into cerebral oxygen balance and multiple processes influencing cerebral blood flow.

Methods We conducted an observational study to assess perioperative oxygen balance. Regional and global saturation, cerebral blood flow velocity, cerebral activity, and vital signs were recorded. Within patients, differences in the supply and demand parameters between hypoxia and normoxia were observed. Differences in performance of autoregulation and neurovascular coupling were also assessed by calculating mean flow index (Mx), correlation between EEG and TCD and by performing transfer function analysis.

Results We included four patients who underwent aortic arch surgery between May and October 2022. Of the total measured data, 84.9% were rejected due to artifacts or desynchronization. Hypoxia was registered in 50% (2/4) of patients. In one patient, both hypoxic and normoxic saturation levels were measured. CBFV and high-frequency EEG powers were lower under hypoxia than under normoxia. Moments of impaired autoregulation were observed in hypoxia. Analysis of neurovascular coupling was inconclusive.

Discussion and Conclusion Our study proves that hypoxia can occur postoperatively. Monitoring cerebral saturation on the intensive care may allow for patient-specific intervention, which may prevent or limit the occurrence of and damage from hypoxia. Conclusions about the progression of oxygen balance cannot be drawn because of the amount of missing data. However, the lowered flow and lowered activity in hypoxia suggest an oxygen imbalance. Future studies should try to obtain consecutive clean data with all modalities simultaneously, so that balance can be assessed. Moreover, saturation measurements should be as consistent as possible so that the duration and severity of hypoxia can be assessed.

Keywords hypoxia – aortic arch surgery – postoperative neurological dysfunction – multimodal monitoring – oxygen balance

Graduation committee

Chairman and technical supervisor	prof. dr. R.J.A. Van Wezel (University of Twente)
Clinical supervisor	dr. C.W. Hoedemaekers, MD (Radboudumc, Nijmegen)
Supervisor personal development	N.S. Cramer Bornemann, MSc. (University of Twente)
Additional member	C.R. van Kaam, MSc. (Radboudumc, Nijmegen)
External member	R.S.P. Warnaar, MSc. (University of Twente)

List of abbreviations

ABP - Arterial blood pressure

ACA - Anterior cerebral artery

C_aO_2 - Content of arterial oxygen

CBF - Cerebral blood flow

CBFV - Cerebral blood flow velocity

$C_{vj}O_2$ - Content of jugular venous oxygen

DAR - Delta-to-alpha ratio

ECC - Extracorporeal circulation

EEG - Electroencephalography

HHb - Deoxygenated hemoglobin

ICU - Intensive care unit

MAP - Mean arterial pressure

MCA - Middle cerebral artery

Mx - Mean flow index

NIRS – Near-infrared spectroscopy

NVC - Neurovascular coupling

O_2EF_{vj} - Jugular venous oxygen extraction fraction

O_2Hb - Oxygenated hemoglobin

OR - Operating room

PND - Postoperative neurological complications

POCD - Postoperative cognitive dysfunction

POD - Postoperative delirium

rSO_2 - Regional saturation

SpO_2 - Global saturation

$S_{vj}O_2$ - Jugular venous oxygen saturation

TCD - Transcranial doppler ultrasound

TFA - Transfer function analysis

TSI - Tissue saturation index

Table of contents

1. Introduction

Despite advancements in surgical techniques and cerebral protection strategies, aortic arch surgery still comes with risks of postoperative neurological complications (PND) [1], [2], [3]. These complications include stroke, postoperative delirium (POD), and postoperative cognitive dysfunction (POCD). Neurological complications affect the quality of life and survival of patients and are associated with an increased length of hospital stay [4], [5], [6]. A mismatch between supply and demand of oxygen in the brain is considered to be one of the most important mechanisms that can lead to cerebral ischemia, with neurological dysfunction as a result. Perioperative multimodal monitoring could give insight into the multiple processes influencing the cerebral blood flow.

1.1. Aortic arch surgery

The aortic arch is the origin of the vessels supplying blood to the brain [7]. The structural integrity of the aorta can decrease, leading to dilatation or aneurysm formation. Aneurysms often develop over the course of many years with little to no symptoms. When left untreated, these aneurysms are at risk of dissection, which is life-threatening.

Aneurysms or dissections are treated with partial or complete replacement of the aortic arch. Depending on the technique and the expected duration of the procedure, cooling is done to 20-25°C centrally. After cooling, circulation is stopped and cerebral perfusion through extracorporeal circulation (ECC) is started. The aorta is then opened and the replacement graft is fitted. Through several anastomoses, the graft and aorta are joined and circulation is reinstated. After rewarming the patient, the operation is completed by closing the wounds. After the procedure, the patient is transferred to the intensive care unit (ICU) for recovery. [8]

Aortic arch surgery is physically demanding and, depending on the location of the repair, usually requires circulatory arrest and adequate cerebral protection strategies. Despite the use of these strategies, there is a significant risk of PND.

1.2. Postoperative neurological complications

Three types of neurological complications commonly found after aortic arch surgery are stroke, POD, and POCD.

Ischemic stroke occurs when cerebral blood flow is interrupted or reduced and ischemia ensues or cardiac emboli interrupt flow in the blood vessels of the brain. After aortic arch surgery, ischemic lesions are found in up to 70% of patients [9], while symptomatic stroke occurs in 7.6 to 16.8% of patients [10], [11], [12].

POD is an acute cognitive disorder that is common after surgery. Patients are characterized by an alteration in the level of attention and awareness from their baseline before surgery. The incidence of POD after aortic arch surgery ranges from 24 to 47% [13], [14], [15] .

While POD presents shortly after surgery, POCD develops in the weeks after surgery and is detectable from the point of expected neurologic recovery, 30 days after surgery [2]. POCD refers to decrements from baseline in a variety of cognitive functions such as attention, concentration, memory, executive function, verbal fluency, and/or visual-spatial performance [3]. The incidence of POCD after aortic arch surgery is approximately 41% [16].

The etiology of PND is multifactorial and can result from the combination of a patient's baseline vulnerabilities and the insults that occur during hospital stay [17], [18]. Two important pathophysiological processes involved are cerebral hypoxia and inflammation [19].

Hypoxia occurs when oxygen demand exceeds supply and this plays a central role in PND [3]. The brain depends on the supply of nutrients and oxygen from the blood to function properly. When cerebral blood flow (CBF) is insufficient, the brain has no reserve and becomes ischemic immediately [3]. Focal brain ischemia most commonly arises from obstruction of arterial blood flow to the brain, often because of stenosis or embolism. The handling of the aorta during surgery is known to disrupt atherosclerotic plaques causing emboli to enter the bloodstream [10]. Similarly, air bubbles can travel towards the brain during surgery and block the blood flow [17]. These bubbles can originate from the manipulations of the ECC system or inside the system as cavitation bubbles [17]. Global ischemia can be caused by cerebral hypoperfusion when mechanisms that control blood pressure are disrupted or perfusion is insufficient. Hypoperfusion can exacerbate the effect of emboli [17].

The severity and effect of ischemic lesions depend on the size and location[3]. While larger lesions are recognized as stroke by clinically obvious symptoms, smaller lesions may appear asymptomatic but can influence cognitive function [3]. For example, injury to the motor cortex may lead to a clinically obvious stroke but a smaller volume of thalamic injury or frontal sub-cortical ischemic injury might only manifest as POCD [3].

Inflammation is another mechanism believed to play a role in PND. Inflammation is triggered through several pathways including hypoxia, tissue trauma, exposure to anesthetic agents, and by use of ECC during the surgery itself [17], [18], [20]. These interventions activate the peripheral inflammatory response which increases production of reactive oxygen species and cytokines, which dysregulate the blood-brain barrier. As this barrier becomes more permeable, peripheral cytokines transverse towards the brain. This further increases the inflammatory response, resulting in a positive feedback loop [20]. In the brain, the cytokines activate microglia and astrocytes which produce central nervous system cytokines and reactive oxygen species. These processes are likely interacting to cause PND by promoting neurotransmitter dysregulation and network dysconnectivity, causing an imbalance in the neural networks [18].

1.3. Multimodal monitoring

Several options for neuromonitoring are available, each with its drawbacks and advantages. By combining multiple techniques, a more complete understanding of the physiology can be acquired [1], [2]. While advantageous, multimodal monitoring comes with challenges. Simultaneous recording with different modalities for long periods can be a logistic and practical challenge for operators. Moreover, recording data with different devices raises the challenge of synchronizing the multiple data streams. In this study, near infrared spectroscopy (NIRS), transcranial Doppler ultrasound (TCD), jugular venous oximetry, and Electroencephalography (EEG) are used in addition to parameters obtained from bedside monitoring.

1.3.1. Near-infrared spectroscopy

NIRS is a non-invasive optical monitoring technique that measures the concentrations of oxygenated hemoglobin (O_2Hb) and deoxygenated hemoglobin (HHb) in the brain.

Near-infrared light of 780 and 850nm is produced by a light source that can penetrate the scalp and reach the cortical surface [21], [22], [23]. Light is absorbed and scattered based on different chromophores present in the tissue. Chromophores are molecules that absorb specific wavelengths of light. In the case of NIRS, the dominant absorbing chromophores O_2Hb and HHb absorb both wavelengths in different quantities. Therefore, the scattered light after absorption provides information about the amounts of O_2Hb and HHb in the tissue under the assumption that the absorption from other tissues remains constant [24]. From amount of O_2Hb and HHb the regional saturation (rSO_2) can be calculated. The parameter for rSO_2 is tissue saturation index (TSI).

NIRS has been used in research and clinical practice and has been shown to measure cerebral desaturation with changes in CBF, and physiologic studies have showed validity for the measurement of cerebral oxygenation [2]. In cardiac surgery, NIRS is used to guide adequate perfusion during CPB [25]. A survey of cardiac anesthesiologists showed that 59% use cerebral oximetry monitoring in aortic arch surgery [2].

NIRS devices are usually placed on the forehead to continuously monitor regional saturation in the prefrontal cortex. This represents the most distal tissue supplied by both the anterior cerebral artery (ACA) and middle cerebral artery (MCA), which is the most vulnerable to hypoperfusion [26]. While continuous monitoring is advantageous, it comes at the cost of low spatial resolution when only the prefrontal cortex is monitored. Hypoxic regions outside the NIRS-monitored zone are missed.

1.3.2. Transcranial doppler ultrasound

TCD is a noninvasive technique that can measure cerebral blood flow velocity (CBFV) in the MCA. High-frequency sound waves (2MHz) are sent through the skull and reflect off the blood cells moving through the blood vessels [2]. The frequencies of the reflections differ depending on the direction and speed of the blood, owing to the Doppler effect [27]. Reflections are, therefore, converted into velocities, providing a real-time assessment of CBFV patterns. CBFV is commonly used as a surrogate for CBF, under the assumption that artery diameter remains constant [2]. Measurement of MCA velocity has shown a good correlation with changes in CBF, and a reduced CBFV is associated with cerebral ischemia in patients undergoing carotid endarterectomy [28]. Furthermore, TCD combined with arterial blood pressure (ABP) allows for the assessment of cerebral autoregulation. Assessing the individual limits of autoregulation with subsequently adjusted blood pressures showed improved neurologic outcomes [2].

While the possibilities for non-invasive continuous monitoring are advantageous, TCD also has limitations. Most notably, the CBFV is only a surrogate marker for the flow and the cerebral flow is the parameter of interest. Furthermore, TCD is limited by the required technical skill during use and interpretation, susceptibility to artifacts, and loss of signal [2].

1.3.3. Electroencephalography

EEG monitors the electrical activity generated in the cerebral cortex. Neuronal spiking in the cortex generates extracellular electrical potentials, caused by postsynaptic potentials and neuronal membrane hyperpolarization [29]. The layout of firing pyramidal neurons allows for the production of larger local field potentials because the dendrites of the neurons run parallel to each other and perpendicular to the scalp [30]. EEG measures these potentials between electrodes applied on the scalp. Applying electrode placement according to the international 10-20 system allows for reproducibility and standardized interpretation of signals [31]. The resulting EEG channels display a wide range of frequencies, which are divided into five frequency bands. The frequency of the signals describes the firing pattern of neurons and is associated with different behavioral and neurophysiological states [32]. The five frequency bands are delta (0-4 Hz), theta (4-8 Hz), alpha (8-16 Hz), beta (16-32 Hz), and gamma (>32 Hz).

Reduced oxygen delivery can actively decrease neural activity and EEG slowing, which shows a decrease in the amplitude of higher frequency alpha and beta waves and increases in amplitude of lower frequency theta or delta waves [28]. Further reduction of oxygen results in an isoelectric EEG pattern, indicating extreme suppression of neural activity [2]. The response of EEG to oxygen depletion allows the detection of cortical ischemia [32]. Quantitative EEG indices, which are sensitive to the power of delta relative to faster activity, have proven particularly informative for detection of ischemia [33]. One of these indices is the delta-to-alpha ratio (DAR), which compares delta to alpha band power.

Several observations indicate that continuous monitoring of DAR can aid bedside assessment of the efficacy of acute reperfusion therapies [33], [34], [35]

While EEG changes are specific to ischemia, reliability is tempered by confounding factors. Depth of anesthesia, medications, hypothermia, and pre-existing cortical injury all are confounding factors that limit the sensitivity of EEG for detecting cerebral ischemia [36]. Hypoxic events deeper in the brain will go unnoticed, further limiting sensitivity [28]. Additionally, EEG monitoring is very sensitive to artifacts and interference, and disturbances can make obtaining reliable data difficult. [32]

1.3.4. Jugular venous oximetry

Jugular venous oximetry can provide insight into the global oxygenation of the brain. The technique requires retrograde placement of a bulbus catheter into the jugular venous bulb via the internal jugular vein [28]. Sampling of blood from the catheter permits blood gas analysis of venous blood draining from the brain. Combined with arterial blood gas analysis, jugular venous blood gas analysis allows for the calculation of several parameters of interest, such as the jugular venous oxygen saturation ($S_{vj}O_2$), the content of arterial (C_aO_2) and jugular venous ($C_{vj}O_2$) oxygen, and the global oxygen extraction fraction (O_2EF_{vj}). The O_2EF_{vj} represents the proportion of oxygen extracted by tissue as blood passes through the capillaries. Changes reflect underlying changes in oxygen metabolism of the tissue and can be an indicator of cell stress or death in normal aging or cerebrovascular conditions such as Alzheimer's disease, Parkinson's disease, and ischemic stroke. [37]

1.4. Regulatory mechanisms of cerebral blood flow

Due to the high metabolic rate of the brain, combined with limited energy storage adequate cerebral perfusion is crucial [38]. Hypo- or hyperperfusion will result in a mismatch of oxygen supply and demand. Multiple hemodynamic mechanisms regulate CBF to ensure perfusion is optimal. For the aim of this thesis, cerebral autoregulation and neurovascular coupling will be discussed.

1.4.1. Cerebral autoregulation

Cerebral autoregulation describes the ability of the cerebral vasculature to keep a constant cerebral perfusion despite variations in ABP [38]. Increases in ABP cause blood vessels to constrict raising resistance and reducing flow. Decreases in ABP cause vascular dilatation and increases in CBF. “Static” autoregulation describes the effect of steady-state ABP changes on CBF. The lower and upper limits of autoregulation are variable and can be influenced by factors such as chronic hypertension [38]. “Dynamic” autoregulation is referred to as the ability of autoregulation to adapt CBF in relation to the speed of the ABP change. The autoregulation functions as a high-pass filter (Figure 1) [38]. If the ABP changes quickly, the response in autoregulation lags and it takes time before CBF is corrected. If the ABP changes slowly the cerebral autoregulation maintain stable CBF. While static and dynamic autoregulation are two terms, they both describe the same physiological phenomenon.

Hypoperfusion and ischemia occur at pressures below the lower limit because the autoregulation fails to maintain sufficient perfusion. At pressures above the upper limit, force-mediated dilation occurs, resulting in increased flow, edema, and hyperperfusion. If impaired or lost, the cerebral vasculature is unable to keep CBF stable in the same blood pressure range as before. The plateau as seen in Figure 1a can shift and become smaller, bringing the lower and upper limits closer together. Fully lost autoregulation will have no plateau in which CBF is kept stable. Outside of the range of autoregulation the CBF passively follows changes in ABP, which leads to hypo- or hyperperfusion more easily [38].

Several studies have suggested that autoregulation may be lost during aortic arch surgery and have advocated adequate perfusion pressure management [1], [39]. The function of cerebral autoregulation can be assessed in the time domain as the correlation between the mean arterial pressure (MAP) and CBFV or rSO_2. In the time domain, the mean flow index (Mx) has been used to assess dynamic cerebral autoregulation in several studies with a variety of patient categories, and for some of these, a poor outcome has been linked to more profoundly disturbed autoregulation [40].

Intact autoregulation is indicated by an Mx of approximately zero (CBF and MAP are not correlated). Impaired autoregulation is indicated by an Mx approaching +1 (CBF correlates and passively follows MAP). There is currently no consensus on the exact cutoff, and cutoffs may vary between patients [41].

To study autoregulation in the frequency domain, transfer function analysis (TFA) is performed. TFA is based on the concept that autoregulation minimizes the effect of ABP oscillations on CBFV [38], [42]. With completely impaired autoregulation each oscillation in ABP would cause an oscillation of a similar duration, magnitude, and frequency in CBFV. Assuming the autoregulation behaves like a linear control system, TFA expresses the relation between the input (ABP) and output (CBFV) in coherence, gain, and phase.

The gain presents the relative power between the signals, with higher gain corresponding to a larger effect of the ABP on the CBFV. The phase represents the timing between the signals, thus quantifying the shift in time of the ABP compared to the CBFV. The coherence represents the fraction of output (CBFV) that is linearly explained by the input (ABP) [42].

TFA is applied over three frequency bands: very low frequencies (VLF), low frequencies (LF), and high frequencies (HF) corresponding to 0.02-0.07 Hz, 0.07-0.20 Hz, and 0.20-0.50Hz respectively. These frequency bands show different characteristics in gain, phase, and coherence, as described in the CARnet study [43].

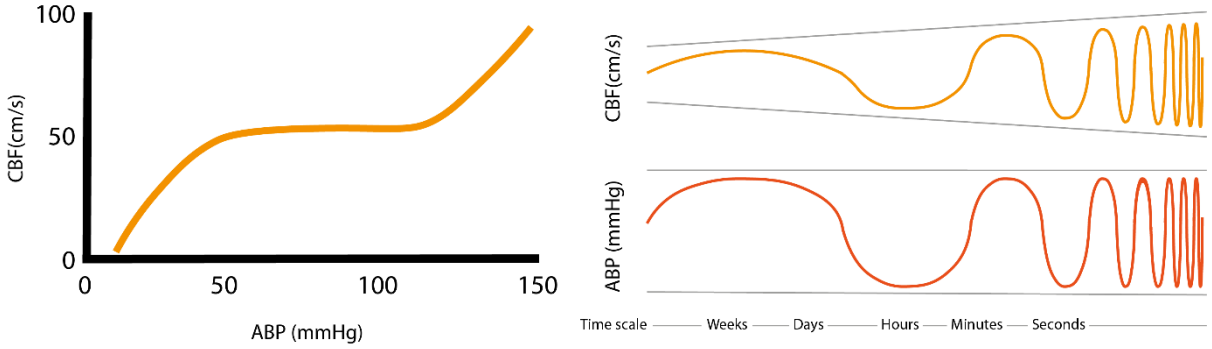

Figure 1: On the left side, the static autoregulation with on the horizontal axis arterial blood pressure (ABP) and on the vertical axis cerebral blood flow (CBF). Between 50 and 110 mmHg the CBF is kept constant, despite rising ABP. Outside of these ranges, the CBF follows the ABP passively. On the right side, is the effect of dynamic autoregulation. On the horizontal axis is a time scale and on the vertical axes, CBF in blue and ABP in red are visualized. Very slow changes in ABP have little effect on the amplitude of the CBF, while quick changes have a large effect. Figure adapted from Claassen et al. [38]

1.4.2. Neurovascular coupling

Neurovascular coupling (NVC) describes the adaptation of CBF to changes in cerebral metabolism [44]. The neurovascular unit is a complex structure that consists of endothelial cells, neurons, smooth muscle cells, pericytes, and astrocytes. The cells of the neurovascular unit sense changes in local neuronal activity and cause changes in local blood flow, mediated by transmission through astrocytes [45]. In the absence of active NVC, an increase in neuronal activity will not be accompanied by an increase in cerebral blood flow and cerebral supply and demand will be out of balance, resulting in possible neurological complications [46]. Several risk factors are believed to impair NVC, including stroke, hypertension, hypotension, and increased age [46].

As the EEG contains information on neural activation and TCD allows for insight into CBF supply, combining EEG and TCD allows for insight into NVC. As CBF should increase with increases in activity, CBFV and the DAR should show a correlation. As the DAR is expected to decrease with increases in activity, the correlation between the CBFV and DAR is expected to be negative.

1.5. Hypothesis

A mismatch between the supply and demand of oxygen in the brain is considered to be one of the most important pathways that can lead to cerebral ischemia, with neurological dysfunction as a result. Perioperative multimodal monitoring could give insight into the multiple processes influencing the cerebral blood flow.

In this thesis, we focus on monitoring the balance between supply and demand of cerebral oxygen. We focus on the peri-operative occurrence of hypoxia. Patients go into surgery without brain injury and during or after the procedure they can develop neurological complications. We hypothesize that during or after the procedure moments of oxygen disbalance can occur, resulting in lowered regional saturation in the brain. As a primary objective, we aim to study the change in regional cerebral saturation through NIRS and jugular venous oximetry. At moments of hypoxia, we want to study the balance between supply and demand. Supply will be measured as cerebral blood flow velocity in the middle cerebral artery measured through TCD. Demand is quantified by the electrical activity in the cortex measured through EEG. As a secondary objective, we aimed to study underlying cerebrovascular mechanisms of cerebral autoregulation and neurovascular coupling at moments of disbalance. We suspect that these mechanisms may be altered during these moments.

2. Synchronization issue

The test setup simultaneously collected NIRS, TCD, and bedside monitor parameters on a single computer and merged these data streams in the Intensive Care Monitor software (ICM+, Cambridge Enterprise, University of Cambridge, U.K.). Data from the bedside monitor imported into ICM+ showed moments of data loss. ABP, ECG, and global saturation (SpO_2) dropped instantaneously to -99999 and returned to physiological values shortly after. The TCD and NIRS signals in the ICM+ file did not exhibit this behavior. After ABP and ECG returned, phase shifts were observed between the ABP and TCD signal. Figure 2 shows the data gaps and their effects on data synchronization. The occurrence of these data gaps appeared irregular in frequency and could be seen in all datafiles of this study. The effect of these data gaps on the synchronization between bedside monitor parameters, NIRS, and TCD was unknown.

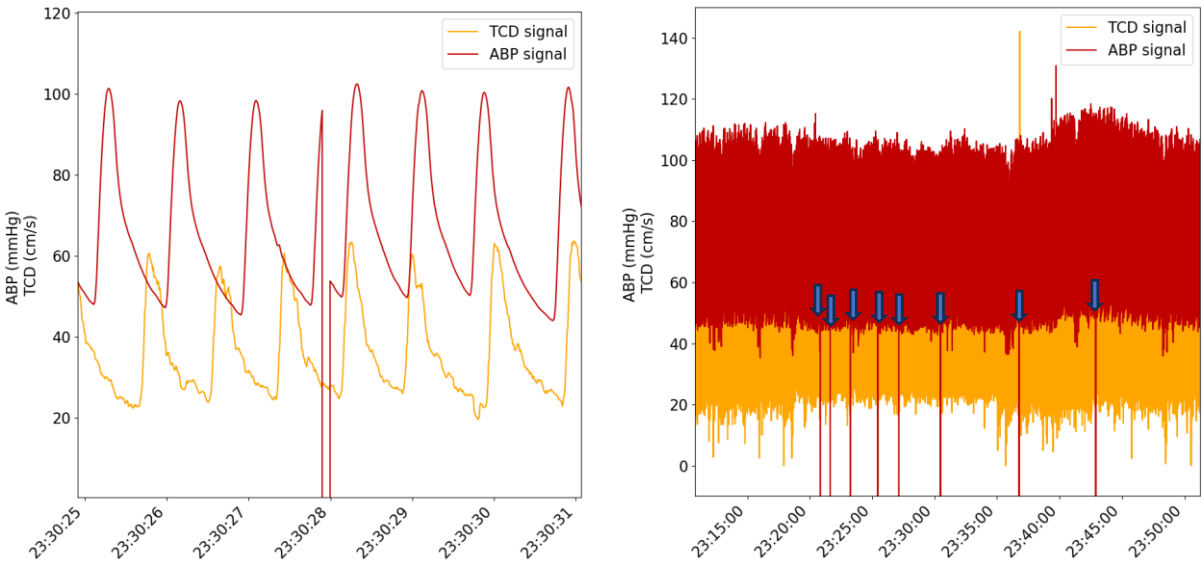

Figure 2: Occurrence of the data gaps over time and their effect. On the left, a data gap is present in the arterial blood pressure (ABP), while the transcranial Doppler (TCD) signal remains unaffected. At least one beat is lost, and a phase shift is visible. On the right, eight data gaps (marked with blue arrows) are present in the ABP signal over a 25-minute timespan.

Due to the shifts in bedside monitor data, it was unclear whether data of the ICM+ dataset was still synchronized with the NIRS dataset in Oxysoft (3.0.103.3, Artinis Medical Systems, Elst, The Netherlands) and the EEG dataset in BrainRT. Figure 3 shows an overview of the monitoring setup and its data streams. Two problems appear in the overview: data gaps appear in data from the bedside monitor (1) and possible desynchronization of NIRS between ICM+ and Oxysoft datafiles (2).

From our setup, three data files were produced. All three files should be synchronized based on the internal clocks of both computers (Figure 3) as both computers had been synchronized with local area network time before measuring. The TSI parameter was calculated in Oxysoft, giving the need for good synchronization between Oxysoft and ICM+ data. While NIRS was imported into ICM+, the method ensured only importing of O_2Hb and HHb averages and not waveforms or TSI waveforms. To test synchronization, O_2Hb from the ICM+ and the Oxysoft dataset were inspected.

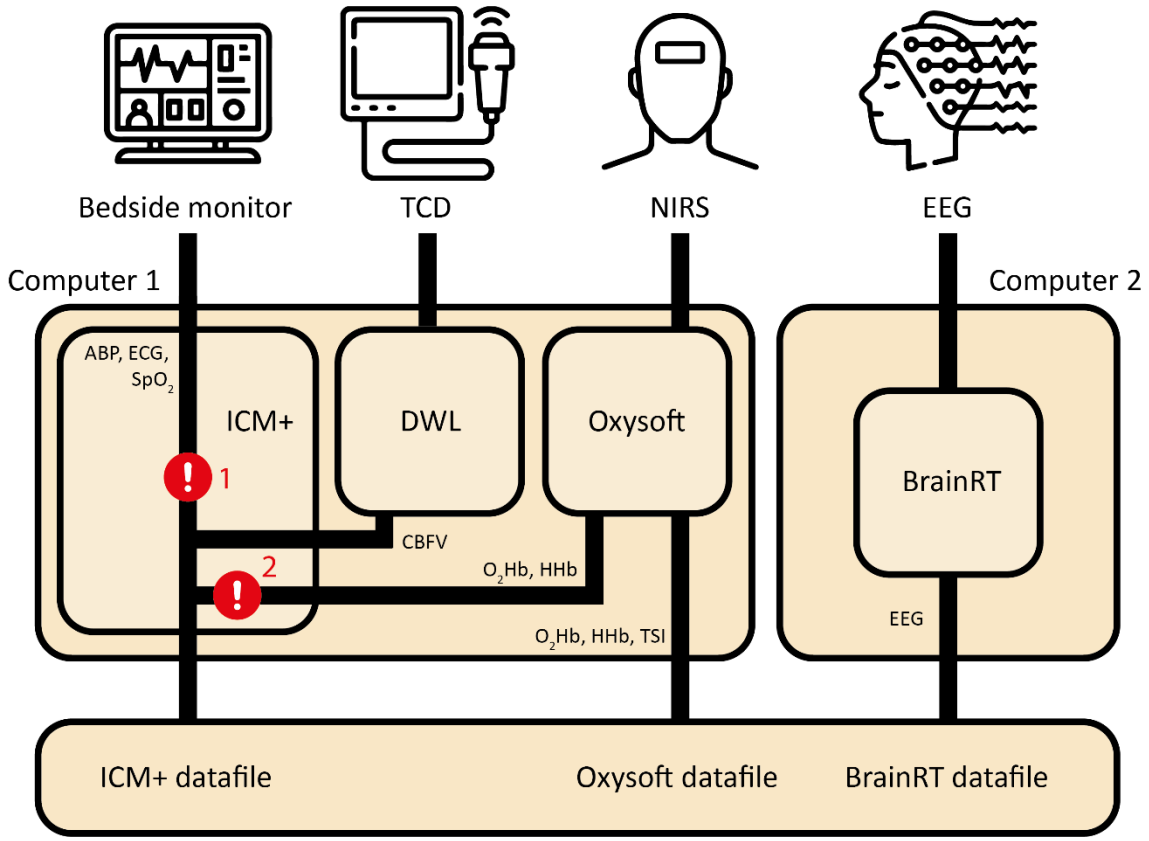

Figure 3: An overview of the monitoring setup. Bedside monitor parameters, transcranial Doppler (TCD) data, and near-infrared spectroscopy (NIRS) data are collected by computer 1. Arterial blood pressure (ABP), electrocardiogram (ECG), and saturation (SpO_2) are streamed directly into ICM+ via the RS232 cable. In this data, problem 1: the data gaps occur. TCD data is collected in the DWL software, and the cerebral blood flow velocity (CBFV) is streamed to ICM+. NIRS data is collected by the Oxysoft program and O_2Hb and HHb are streamed to ICM+ as averaged values. Here occurs problem 2: O_2Hb in the ICM+ dataset was asynchronous with the Oxysoft dataset.

2.1. The scope of the problem

Figure 4 displays the frequency of data gaps over time and the difference in phase between heartbeats for one of the recordings at the ICU. On the left, a gap length of 0.256 seconds can be observed regularly, but the gap length is otherwise random. This semi-regular occurrence of data gaps of length 0.256 seconds was observed in five out of eight recordings. On the right, the difference in phase between the ABP and CBFV waves before and after the data gap is plotted against the length of the data gaps. Note that a shift with the duration of one or multiple heartbeats, would appear as a phase shift of 0 and this method only illustrates the variability of the effect of the data. This analysis confirmed the suspicion that the occurrence and effect of data gaps were unpredictable, despite the presence of a semi-regular pattern.

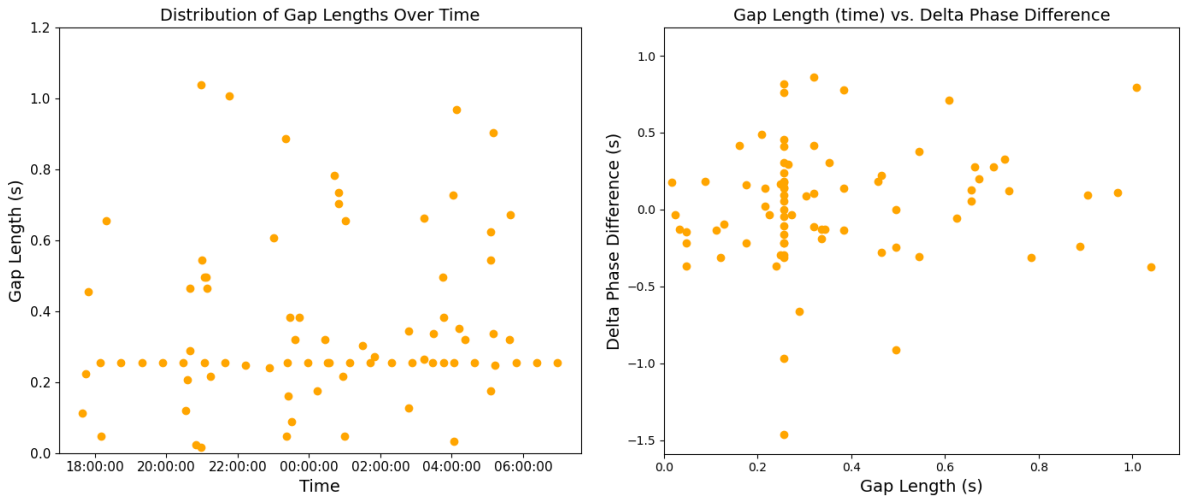

Figure 4: On the left, the occurrence of data gaps and gap length over time. On the horizontal axis, the time of recording in the ICU is shown. On the vertical axis, the gap length in seconds shows how long data appears to be missing. In the right graph, the effect of gap length on phase shift between beats before and after the gaps.

Table 1 shows the occurrence of the data gaps for all recordings. The average time between data gaps was 7 minutes and 5 seconds overall recordings. Data gaps occurred more regularly in the OR, on average every 5 minutes and 3 seconds. In the ICU the gaps occurred every 9 minutes and 38 seconds. The overview of the occurrences shows high variability in frequency between recordings, further confirming the irregularity of the data gaps. The high number of gaps per measurement strengthens the suspicion that small phase shifts could possibly add up to a substantial phase shift between data from the bedside monitor and other data streams.

Table 1: An overview of the occurrence of data gaps. The amount, median gap length, total duration of the recording, and frequency of gaps over time are shown per patient. OR: operating room, ICU: intensive care unit

	Patient 1		**Patient 2**		**Patient 3**		**Patient 4**	
	OR	*ICU*	*OR*	*ICU*	*OR*	*ICU*	*OR*	*ICU*
Amount	68	115	59	67	69	156	64	80
Median gap length (s)	0,256	0,320	0,256	0,256	0,256	0,288	0,248	0,256
Recording duration	05:36:51	15:43:39	05:29:03	15:38:09	04:56:44	14:59:53	03:03:44	14:02:14
Gaps/time	00:04:57	00:08:12	00:05:35	00:14:00	00:04:18	00:05:46	00:02:52	00:10:32

2.2. The relevance of the data gaps

The phase shift caused by the data gaps caused a problem in the data analysis. In TFA, phase shift is one of the outcome measures, and multiple data gaps in a recording could result in a larger phase shift, influencing outcomes. Variations in correlation due to desynchronization could influence Mx outcomes because the Mx measures correlation between the ABP and CBFV. Furthermore, desynchronization between the ICM+ and Oxysoft, and BrainRT software would be problematic as the TSI from the Oxysoft dataset was linked to the TCD parameters from the ICM+ dataset. As this study is part of a larger observational study, guaranteeing data quality was crucial. Therefore, inclusion of new patients had to be postponed until this problem was resolved.

2.3. The cause of the data gaps

While the data gaps occurred in the ABP signal, it was possible that NIRS and/or TCD were causing problems in ICM+ that resulted in ABP desynchronization. It was therefore important to rule out influences of the different techniques on the problem. This included the possible influence of a fault in the RS232 cable or differences between bedside monitor models.

We performed 20 measurements in different setup combinations, after which it became clear that without the involvement of other techniques, data gaps were present. Table 2 shows an overview of the setup combinations. The cable or monitor model did not influence the occurrence of data gaps. We concluded that the problem lay in the communication between the bedside monitors and the incoming data stream into ICM+.

Table 2: An overview of the different setup combinations. TCD: transcranial Doppler, NIRS: near-infrared spectroscopy, ICM+: intensive care monitoring software

Setup combination	Goal	Outcome
Bedside monitor parameters, TCD, and NIRS in ICM+. NIRS in Oxysoft	Test the occurrence and frequency of data gaps	Data gaps present in ICM+ file
Bedside monitor parameters, and NIRS in ICM+. TCD running in DWL. NIRS in Oxysoft.	Rule out TCD influence	Data gaps present in ICM+ file
Bedside monitor parameters, and NIRS in ICM+. TCD turned off. NIRS in Oxysoft.	Rule out TCD influence	Data gaps present in ICM+ file
Bedside monitor parameters, and TCD in ICM+. NIRS running in Oxysoft	Rule out NIRS influence	Data gaps present in ICM+ file
Bedside monitor parameters, and TCD in ICM+. NIRS turned off	Rule out NIRS influence	Data gaps present in ICM+ file
Bedside monitor parameters in ICM+	Test if gaps are present without NIRS and TCD	Data gaps present in ICM+ file
Bedside monitor parameters in ICM+, using a different RS232 cable	Rule out influences of the RS232 cable	Data gaps present in ICM+ file
Bedside monitor parameters in ICM+, using a MP70 monitor model	Rule out influences of the monitor model	Data gaps present in ICM+ file
Bedside monitor parameters in ICM+, using a MX800 monitor model	Rule out influences of the monitor model	Data gaps present in ICM+ file

2.4. Solving the problem

2.4.1. Software updates to ICM+

We contacted the developers of the ICM+ program. After sending initial data and elaborating on the data gaps problem, tests were run to solve the problem. Between July and November 2023, another 22 tests were run in cooperation with the developers. Software updates and configuration profiles for ICM+ were provided for each test. The software updates were provided to improve ICM+, while the configuration profiles were constructed to give the developers insight into the metadata of the program. Some tests were run with TCD and/or NIRS, while others were run with just the bedside monitor. After each test, data and metadata were sent to the developers. After the last test on November 29, we received confirmation from the developers of the ICM+ program that the problems had been resolved. This makes it possible to restart patient inclusions without desynchronization or data loss.

2.4.2. Time axis comparison between the ICM+ and Oxysoft datasets

Due to the phase shift from the data gaps, it was not known if the ICM+ data would still have the correct synchronized time. To verify the synchronization between the ICM+ and Oxysoft datasets, O_2Hb of both datasets were visually inspected. Time shifts were determined based on morphology of the signals. There was a time shift between Oxysoft and ICM+ O_2Hb visible between 0 and 12 seconds all but one datafile. Notably the time shift varied within files, often increasing with the duration of the measurement. In the remaining datafile, a time shift of 31 minutes and 50 seconds was observed (see Figure 5). This file also showed differences in O_2Hb, even when corrected for time shift. This may possibly be due to the method of importing NIRS into ICM+. While TCD data is imported as raw waveforms, NIRS data is imported as averaged data. While Oxysoft collects data at 50Hz, the data stream in ICM+ is averaged and down sampled to 1Hz. It is unknown whether this difference in importing method between TCD and NIRS was the cause of the difference between NIRS and Oxysoft O_2Hb data.

To correct for the time shifts, raw and ICM+ data were plotted and the ICM+ data was shifted to line up with the raw data based on the morphology of the signal. The same time shift was performed on the whole ICM+ datafile, also shifting the CBFV.

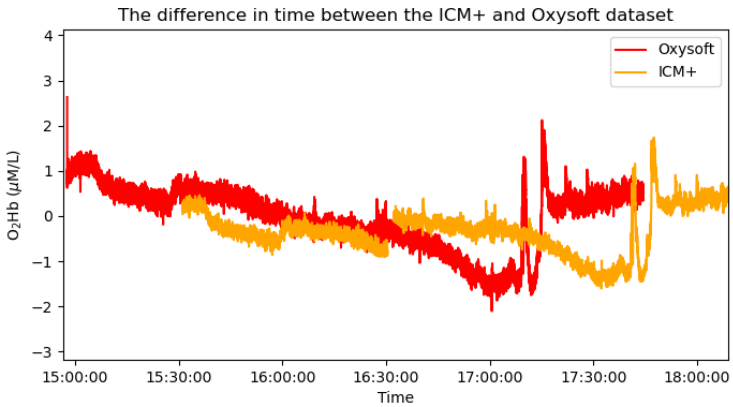

Figure 5: The comparison between the ICM+ and Oxysoft dataset. A time shift of 31 minutes and 50 seconds between raw near-infrared spectroscopy (NIRS) (red) and ICM+ NIRS (blue) is visible. Note the differences in O_2Hb and the jumps in the ICM+ dataset.

2.4.3. Repair of the original dataset

To allow for TFA and calculation of the Mx, resynchronization of existing data was necessary. To achieve resynchronization, we received help from Nick Eleveld MSc. at the UMCG [47]. At the UMCG a novel algorithm had been developed to synchronize the ABP and TCD data based on their correlation. Both signals were high pass filtered with cutoff at 0.5Hz to remove drift. Based on the correlation a time shift between signals was calculated and by compensating for the time shift data was resynchronized. The presence of heartbeats was necessary for the functioning of the algorithm. This meant that during ECC data could not be synchronized. Data gaps as well as other artifacts caused a drop in correlation and therefore a variable time shift. Therefore, data could not always be synchronized due to poor signal quality.

After receiving the resynchronized data from the UMCG, data was visually inspected to check if the synchronization was successful. Data was included if artifact-free and the time shift between ABP and TCD was corrected. 6 out of 8 total datafiles (2 per files per patient) allowed for TFA as there were more than 10 minutes of consecutive resynchronized data. In one file, TFA was only possible after combining two segments of resynchronized data and in the final file, TCD quality was insufficient. The maximum time shift between ABP and TCD data was up to 12 seconds, showing the significance of desynchronization and the necessity for repair.

In this study, the resynchronized data was used in the calculation of the Mx and TFA, due to the need for ABP which were affected. All other calculations were performed on original data that didn't show data loss.

3. Methods

3.1. Study design and population

We performed an observational trial in adult patients undergoing elective open aortic arch surgery. This study was approved by the Committee on Human Research (CMO) and registered as file NL76089.091.20. Exclusion criteria were a rescue or emergency procedure, history of neurological disease (known to influence cerebral blood flow and oxygenation), and failure to obtain informed consent.

3.2. Data acquisition

Demographic and clinical data were collected. Measurements were started after induction of anesthesia and continued during surgery and at the ICU. NIRS, TCD EEG, and parameters from the bedside monitor were collected continuously from the start of the anesthesia until 06:00 the next morning in the ICU. Blood samples were collected from the jugular bulb catheter and arterial catheter at the start of anesthesia, during ECC, end of surgery, upon admission at the ICU, and at 20:00PM, 00:00AM, and 06:00AM the next morning (Figure 6).

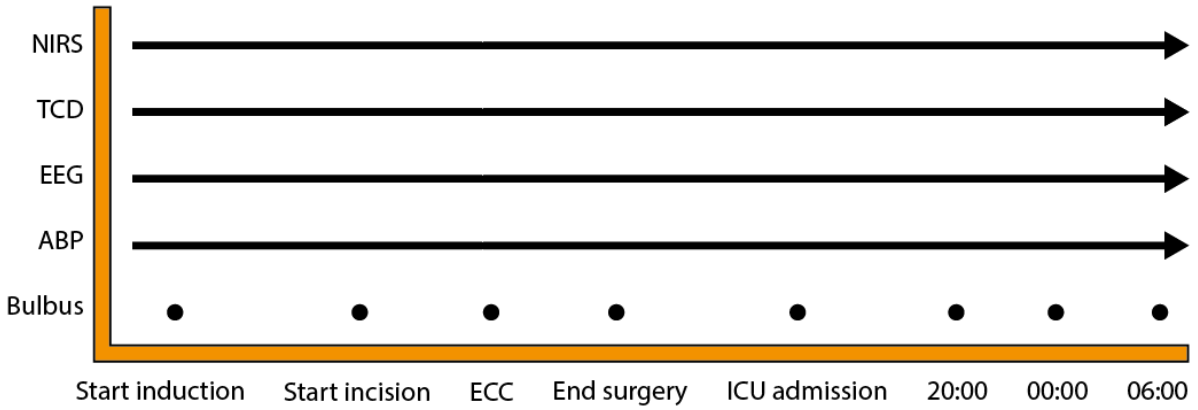

Figure 6: Moments of measuring. NIRS, TCD, and EEG were monitored continuously, while bulbus samples were taken on predetermined moments. NIRS: near-infrared spectroscopy, TCD: transcranial doppler, EEG: electroencephalogram, ECC: extracorporeal circulation, ICU: intensive care unit

The NIRS device (Artinis Medical Systems, Elst, the Netherlands) was placed on the forehead and data was recorded in the Oxysoft program (3.0.103.3, Artinis Medical Systems, Elst, The Netherlands).

TCD of the MCA was performed with a Multi-Dop T device (DWL, Compudemics Germany GmbH). Two 2 MHz probes were aimed through the temporal window and fixated on a head frame.

Parameters from the bedside monitors, such as ABP, ECG, and SpO_2, were imported through a RS232 cable. The Philips InteliVue MP70 and MX800 bedside monitors are used in the ICU of the Radboudumc. In the OR the MX800 model is used.

EEG was performed by placing nine silver-chloride cup electrodes one the scalp 10-20 following the international 10-20 system (O1, O2, T3, C3, Cz, C4, T4, F1 & F2). The FP1 and FP2 positions were inaccessible due to the placement of the INVOS, BIS, and Portalite electrodes. Therefore, F1 and F2 were used instead. Data was recorded in the BrainRT program.

Arterial and jugular blood samples were collected for blood gas analysis from a 7-Fr single-lumen catheter inserted with the tip into the jugular bulb. Monitoring of blood pressure and arterial blood sampling was performed with the use of a catheter in the radial artery.

3.3. Synchronization approach

To ensure synchronization of data streams, the NIRS and TCD programs ran on the same computer as the Intensive Care Monitor software (ICM+, Cambridge Enterprise, University of Cambridge, U.K.) and these data streams were combined with data from the bedside monitor and simultaneously collected in one ICM+ file (Figure 3). TCD was imported as raw waveform data, whereas O_2HB and HHb were imported as average values over time. To ensure synchronization with the EEG dataset, which was obtained with a different computer, the internal time of both computers was synchronized with local area network time. The TSI parameter was calculated in the Oxysoft program retrospectively, meaning this parameter could not be imported into ICM+.

3.4. Monitoring approach

To study the occurrence of hypoxia, regional saturation was measured using NIRS. A decrease in TSI of more than 10% from baseline or a saturation below 50% for 5 minutes or longer was defined as hypoxia [2], [26]. Baseline TSI was defined as the maximum TSI in the period between induction of anesthesia and surgical incision.

For the primary objective, TCD and EEG data were assessed during segments where NIRS, TCD, and EEG were simultaneously present, to gain insight into supply and demand. For the secondary objective, resynchronized ABP and TCD data were assessed when NIRS was present.

To evaluate oxygen supply, mean CBFV was used. A higher velocity suggests a higher flow and therefore a higher oxygen supply. To evaluate the oxygen demand, EEG power was used. A higher EEG power in higher frequency bands suggests more neural activity and therefore more oxygen consumption. The frequency content was evaluated through the EEG band powers. From the frequency band power, the DAR was calculated. To study the balance between oxygen supply and demand the O_2EF_{vj} was calculated.

3.4.1. Near-infrared Spectroscopy

The parameter of interest for NIRS was regional cerebral oxygen saturation (rSO_2), measured as the TSI [48]. Low TSI is a sign of hypoxia. This parameter describes the ratio of O_2Hb to total Hb, calculated as:

$$TSI = \frac{O_2Hb}{O_2Hb + HHb} \quad (1)$$

In this study, averages were calculated over 30-second windows with 50% overlap. As most hemoglobin within the head lies in the venous compartment, a normal rSO_2 is around 70%, with a range of 50% to 75%, with the assumption of a fixed venous-to-arterial ratio [26]. Inter-individual variability has been demonstrated in healthy volunteers, and a meta-analysis of preoperative rSO_2 in cardiac surgery patients found a 95% reference range of 51% to 82%, with a mean baseline of approximately 66% [26].

3.4.2. Transcranial doppler ultrasound

The mean flow velocity can be derived from the CBFV by averaging over time. In this study, average CBFV was calculated over 30-second windows with 50% overlap. Under the assumption that artery diameter remained constant, CBFV was used as a surrogate for CBF [27]. A higher velocity suggests a higher flow rate, and therefore, a higher supply of blood and oxygen. The normal range of mean CBFV is between 49.6 – 56.6 cm/s [49]. In this study, TCD was applied bilaterally to the MCA to assess the oxygen supply. The bilateral approach can be used because asynchrony in the CBFV between hemispheres can indicate stenosis or hypoperfusion [28]. In this study, however, the bilateral approach was chosen to improve the chance of a data stream with sufficient data quality.

3.4.3. Electroencephalography

EEG was used to provide insight into the demand for oxygen. The raw data in the EEG dataset was re-referenced in a bipolar longitudinal montage. The frequency content was evaluated with the use of average spectrograms over all channels. Powers per frequency band were averaged over 30-second windows with 50% overlap. Different levels of cortical activity generate different frequencies and EEG power levels. Higher EEG power in higher frequency bands suggests greater neural activity and increased oxygen consumption [32]. This allowed for the use of EEG power as a surrogate for oxygen demand. The relative frequency band power was calculated for all frequency bands according to:

$$EEG\ band\ power(\delta,\theta,\alpha,\beta,\gamma) = \frac{Frequency\ band\ power(\delta,\theta,\alpha,\beta,\gamma)}{Total\ EEG\ power} \quad (2)$$

From the EEG band power, the delta-to-alpha ratio was calculated as:

$$DAR = \frac{EEG\ power\ \delta}{EEG\ power\ \alpha} \quad (3)$$

3.4.4. Jugular venous oximetry

The $S_{vj}O_2$ measures global oxygenation, with a normal range of 55% to 75%. The $S_{vj}O_2$ has a high specificity, but a low sensitivity for focal ischemia [2]. Despite the low sensitivity for focal ischemia, the $S_{vj}O_2$ was used to test the agreement between NIRS and jugular venous oximetry. A $S_{jv}O_2$ lower than 50% suggests inadequate cerebral oxygenation, due to increased demand or decreased supply [2]. When cerebral demand exceeds supply, the saturation decreases as oxygen extraction increases.

The C_aO_2 and $C_{vj}O_2$ were calculated with the following equations:

$$CaO_2\ (ml\ *dl^{-1}) = [Hb] * 1.36 * \frac{SaO_2}{100} + 0.003 * PaO_2 \quad (4)$$

$$CvjO_2\ (ml\ *dl^{-1}) = [Hb] * 1.36 * \frac{SvjO_2}{100} + 0.003 * PvjO_2 \quad (5)$$

with 1.36 as the constant describing the amount of oxygen bound per gram of hemoglobin and the constant 0.003 representing the amount of oxygen dissolved in plasma. Note that the C_aO_2 was calculated with S_aO_2 and P_aO_2 which are derived from arterial blood gas samples. The arterial and jugular venous oxygen contents were used to calculate the O_2EF_{vj} [50]. The oxygen extraction fraction is the ratio of extracted oxygen to arterial oxygen content. In this study, the parameter gave insight into the balance between supply and demand. A normal O_2EF_{vj} is around 38%. A higher O_2EF_{vj} suggests more oxygen supply than demand and a lower O_2EF_{vj} suggests higher demand than supply. The O_2EF_{vj} can be calculated using:

$$O_2EF_{vj}\ (\%) = \frac{CaO_2 - CvjO_2}{CaO_2} * 100\% \quad (6)$$

3.5. Data preprocessing

Data was preprocessed and analyzed with Python 3.11.4 (Python Software Foundation, Wilmington, Delaware, United States).

NIRS data in Oxysoft had an initial sampling frequency of 50 Hz. TCD from the ICM+ dataset was resampled in the program from 100Hz to 125Hz.

NIRS was first visually inspected for artifacts. Short periods (up to three beats) of large artefacts, where the physiological waveforms were distorted, were removed, and replaced by linearly interpolated values. After interpolation of the NIRS, artifact-free segments of minimally 5 minutes were included for the primary objective, and segments of minimally 10 minutes were included for the secondary objective. If data segments had more than the minimum amount of data, the full artifact free segment was included. Selected segments were saved for further processing.

Then, ICM+ and Oxysoft data were checked for sufficient synchronization. Synchronization between the Oxysoft and ICM+ NIRS datasets was considered sufficient if the time shift was less than 5 minutes and did not cause a segment to switch from label normoxia to hypoxia or vice versa. If necessary, ICM+ data was adjusted to the Oxysoft time axis in accordance with chapter 2 for both the primary and secondary objectives.

TCD and EEG data were visually inspected for artifacts for the primary objective. For the secondary objective, resynchronized TCD and ABP were inspected for artifacts and successful synchronization. Short periods (up to three beats) of large artifact, where the physiological waveforms were distorted, were removed, and replaced by linearly interpolated values.

The EEG was filtered with a bandpass filter with a low cut-off of 0.5 Hz and a high cut-off of 45 Hz. Afterward, artifacts from cardiac activity and eye movements were eliminated with the use of a two-stage adaptive filter based on the method of Correa et al (2007) [51]. The frequency content was evaluated with the use of average spectrograms over all channels. The power spectral density was computed according to Welch's method. A Hann window of 20 seconds was chosen to obtain a frequency resolution of 0.1 Hz. By moving the Hann window across the signal with an overlap factor of 50% the spectrograms were computed. The band power and DAR were calculated using formulas 3 and 4 respectively.

For the secondary objective, minimally 10 minutes of artifact-free data was necessary. Preprocessing for the Mx and TFA was performed in accordance with the recommended methodology [41], [52], [53].

To improve the number of datapoints for TFA, segments longer than 20 minutes were put into 20-minute windows with 80% overlap. A 20-minute window was chosen as a balance between quality and quantity of analysis. Data segments between 10 and 20 minutes were analyzed without windowing. Raw CBFV and ABP waveforms were converted into beat-to-beat data. All beat-to-beat data was then linearly interpolated and resampled at 5Hz to obtain equidistant data points. After creating equidistant data points filtering data was not recommended, but the mean value was removed from each segment [52].

In the calculations for the NVC, EEG was preprocessed and divided into frequency bands as described under the primary objective. Short periods (up to three beats) of large artifact, where the physiological waveforms were distorted, were removed, and replaced by linearly interpolated values.

3.6. Data analysis

3.6.1. Parameters over time

The incidence of hypoxia in time was evaluated by inspecting mean TSI, CBFV, and relative EEG powers per frequency band over time.

3.6.2. The NIRS versus the jugular venous oximetry

Jugular venous oximetry measurements within an hour of available NIRS segments were included. The average TSI within the hour of the jugular venous oximetry measurement was calculated and evaluated against the $S_{vj}O_2$.

3.6.3. Altered supply and demand in hypoxia

Comparison of supply and demand was done within patients and not between patients, due to the low number of patients. For each preprocessed window, TSI were compared against baseline values. TSI lower than 10% from baseline or TSI below 50% were classified as hypoxic. Otherwise, the window was classified as normoxic. Mean CBFV, DAR and EEG power per band were classified as hypoxic or normoxic based on the TSI at that time. TSI values within an hour of taking the jugular venous oximetry measurement were averaged and evaluated against the O_2EF_{vj}.

3.6.4. Cerebral autoregulation

Cerebral autoregulation was analyzed through the calculation of the Mx and through TFA.

3.6.4.1. Mean flow index

For calculating the Mx, we used the most common approach as described by Olsen et al. [41], [54]. The ABP and CBFV were time-integrated as non-overlapping 10-second mean values [55]. This was done to eliminate high-frequency noise from the respiratory and pulse frequencies while allowing oscillations that occur below 0.05 Hz to remain. TCD and arterial ABP waveforms were then high pass filtered with a cutoff set at 0.003 Hz. This removes slow drifts while maintaining the frequencies of interest. A continuous, moving Pearson's correlation coefficient was calculated between the MAP and TCD blood flow velocities giving the Mx. [41], [54], [55]

$$Mx = \frac{\sum(MAP_i - \overline{MAP})(CBFV_i - \overline{CBFV})}{\sqrt{\sum(MAP_i - \overline{MAP})^2(CBFV_i - \overline{CBFV})^2}} \quad (7)$$

From the selected data segments consecutive, paired, 10-second averaged values from 300-second windows with 80% overlap were used for each calculation, incorporating 30 data points per calculation of the Mx. In other words, 5 minutes of data was used for each Mx calculation and 5 minutes were chosen as a balance between good results and data availability.

A cutoff of 0.45 for intact versus impaired autoregulation was chosen, matching the methodology of Brady et al. [55].

3.6.4.2. *Transfer function analysis*

For performing TFA, we followed the methodology from the Updated White paper by Panerai et al. [52]. Preprocessed data was put into Hanning windows of 102 seconds with 50% overlap. The auto and cross spectra were calculated and smoothed with a [1/4,1/2,1/4] triangle filter. The transfer function was then calculated according to the formula[56]:

$$H(f) = S_{xx}(f) * S_{yy}(f) \tag{8}$$

where S_{xx} is the autospectrum of the ABP, $S_{yy}(f)$ as the autospectrum of the CBFV, and S_{xy} the cross spectrum between ABP and CBFV. The gain was then calculated by using the real (H_r) and imaginary (H_i) part of the transfer function

$$|H(f)| = \sqrt{|H_r(f)|^2 + |H_i(f)|^2} \tag{9}$$

The phase was calculated as

$$\phi(f) = \tan^{-1}\left[\frac{H_i(f)}{H_r(f)}\right] \tag{10}$$

and the coherence was calculated as

$$MSC\ (f) = \frac{\left|S_{xy}(f)\right|^2}{S_{xx}(f) * S_{yy}(f)} \tag{11}$$

TFA was applied over three frequency bands: very low frequencies, low frequencies and high frequencies corresponding to 0.02-0.07 Hz, 0.07-0.20 Hz and 0.20-0.50Hz respectively. The complete frequency dependence of coherence, gain and phase in the range 0.02–0.50 Hz were analyzed. Furthermore, the three frequency bands were analyzed separately as well. Coherence, phase, and gain were compared between moments of hypoxia and normoxic control moments.

3.6.5. Neurovascular coupling

NVC was analyzed through calculating the cross correlation of the DAR and the CBFV. EEG power per band and DAR were calculated according to equations 2 and 3 respectively. 10s averages with 90% overlap were calculated over the EEG band powers and the CBFV. The selected data segments were divided in 30s windows with 50% overlap. For each window a cross correlation was calculated between the EEG power per frequency band and CBFV. The DAR was inversed, as we expected a negative correlation. The maxima of the cross correlations per window were compared between moments of hypoxia and normoxic control moments.

3.7. Statistical analysis

All statistical analysis was performed using Python 3.11.4 (Python Software Foundation, Wilmington, Delaware, United States).

All data was continuous and no data was categorical. For the insight into the relation between TSI and supply and demand parameters scatterplots were constructed, and a linear regression curve was fitted. For comparison of parameters between hypoxia and normoxia, histograms were constructed to show the different distributions.

The Shapiro-wilk test was performed to test if distributions were normally distributed [57]. Mean and standard deviations were reported for normally distributed data, while median and interquartile ranges were reported if distributions were not normal. As hypoxic moments and normoxic moments were considered independent from each other, datapoints were considered unpaired.

The Kolmogorov-Smirnov test was performed to test whether the distributions between hypoxia and normoxia differed significantly. The test is a nonparametric statistical test used to assess the goodness of fit between two probability distributions. It tests whether two samples are drawn from the same (but unknown) distribution. The null hypothesis was that samples were drawn from the same distribution. The alternative hypothesis was that samples were drawn from different distributions.

A Bonferroni correction was applied to adjust the significance level as we have conducted multiple analyses based the one hypoxia classification from the TSI. Conducting multiple analyses from the same dataset increases the risk of false positives [58]. The correction was applied according to:

$$Bonferroni - corrected\ p\ value = \frac{Original\ p - value}{Number\ of\ tests} \tag{12}$$

4. Results

4.1. Patient and data characteristics

4.1.1. Patient characteristics

Between May and October of 2022, four patients were included in this study. During this period, a total of 19 patients were screened from which six patients signed informed consent. Due to logistic reasons, e.g., absence of one of the members of the research team, two patients were excluded. From the four included patients, three patients underwent a Bentall procedure, and one underwent a supra coronary aorta ascendens replacement (SCAR) procedure. Only one patient (number 3), developed a delirium during the stay in the hospital. Table 3 illustrates the demographics and clinical data of the included patients. All patients were sedated with the use of propofol and midazolam during surgery.

Table 3: An overview of patient characteristics. Per patient, age, body mass index (BMI), occurrence of postoperative neurological dysfunction (PND), surgery type and durations of surgery, use of extracorporeal circulation and aortic occlusion are shown.

Patient	Gender	Age (yr)	BMI	PND
1	M	57	25.6	-
2	M	78	26.3	-
3	M	66	24.0	Delirium
4	F	82	29.7	-

Patient	Surgery	Surgery time (min)	ECC time (min)	Aortic occlusion time (min)
1	Bentall	307	162	137
2	Bentall	291	149	125
3	Bentall	307	186	141
4	SCAR	207	70	55

Baseline TSI was determined based on stable TSI prior to surgery for all four patients and are shown in Table 4. From this the 10% decrement was calculated resulting in a threshold at 90% of baseline. TSI below this threshold were classified as hypoxia.

Table 4: The baseline tissue saturation indices (TSI) per patient. The 10% decrement from baseline was calculated as a threshold for hypoxia.

Patient	Baseline TSI (%)	TSI 10% from baseline (%)
1	77	69.3
2	75	67.5
3	68	61.2
4	79	71.1

4.1.2. The length of the dataset

The total dataset consisted of 79 hours and 28 minutes based on ICM+ recording time. Data was selected for the primary objective if NIRS, TCD, and EEG were artifact free for more than 5 consecutive minutes. This resulted in a total of 12 hours, 3 minutes and 50 seconds of data used for the primary objective, which is 15.1% of the total dataset. Within this data, hypoxia was measured for a total of 5 hours, 7 minutes, and 40 seconds. Patient 3 and 4 provided 50,2% and 50% respectively of the hypoxic data. Overall, most data were measured in the ICU compared to the OR (Table 5).

Table 5: The duration of the measurements for the primary objective. Durations are taken from the operating room (OR) and on the intensive care unit (ICU) per patient. On the bottom row, the sums of the columns are displayed.

patient	**OR**		**ICU**		**Total**	
	total min	*hypoxia*	*total min*	*hypoxia*	*total per pt*	*hypoxia*
1	00:47:00	00:00:00	00:55:00	00:00:00	01:42:00	00:00:00
2	00:12:00	00:00:00	01:32:30	00:00:00	01:44:30	00:00:00
3	00:19:00	00:05:00	05:44:30	02:28:50	06:03:30	02:33:50
4	00:16:30	00:16:30	02:17:20	02:17:20	02:33:50	02:33:50
	1:34:30	0:21:30	10:29:20	4:46:10	12:03:50	5:07:40

For the Mx calculation and TFA, a total of 8 hours, 13 minutes and 10 seconds were selected of which 3 hours, 24 minutes, and 50 seconds was measured in hypoxia. Again, most data were measured in the ICU compared to the OR (Table 6).

Table 6: The duration of the measurements for the calculation of Mx and for TFA. Durations are taken from the operating room (OR) and on the intensive care unit (ICU) per patient. On the bottom row, the sums of the columns are displayed.

patient	**OR**		**ICU**		**Total**	
	total min	*hypoxia*	*total min*	*hypoxia*	*total per pt*	*hypoxia*
1	01:03:00	00:00:00	01:40:00	00:05:00	02:43:00	00:05:00
2	00:12:00	00:00:00	01:13:50	00:00:00	01:25:50	00:00:00
3	00:26:30	00:12:00	02:51:20	02:21:20	03:17:50	02:33:20
4	00:00:00	00:00:00	00:46:30	00:46:30	00:46:30	00:46:30
	1:41:30	0:12:00	6:31:40	3:12:50	8:13:10	3:24:50

4.1.3. Parameter overview

Table 7 shows an overview of the median, and interquartile ranges for TSI, CBFV, relative alpha power, relative delta power and DAR. Values were reported on the operating room (OR), ICU, and as total over all observations. For the TSI, there are subtle differences between the OR and ICU within patients. Consistent in- or decreases are not visible. For CBFV, within patients 1, 2, and 4 OR velocities are lower than on the ICU. Patient 3, however, has a higher median flow velocity on the OR of 43.8 cm/s compared to its ICU measurements with a median of 38.5 cm/s. The alpha power is higher on the ICU compared to the OR within every patient. The delta power is lower on the ICU compared to the OR within patients, particularly in patient 4. Patient 4 has the highest alpha and lowest relative delta power. For DAR, values have a large range between patients with the highest median 1075.1 on the OR for patient 3, and the lowest median of 1.6 on the ICU for patient 4. The DAR rises with increasing delta power and/or decreasing alpha power.

Table 7: An overview of the median and interquartile ranges of the parameters collected in the operating room (OR) and on the intensive care unit (ICU). OR: operating room, ICU: intensive care unit, TSI: tissue saturation index, CBFV: cerebral blood flow velocity, DAR: delta-to-alpha ratio

	Patient 1			**Patient 2**		
	OR	*ICU*	*Total*	*OR*	*ICU*	*Total*
TSI (%)	75.6 [75.1-76.2]	72.9 [72.7-73.3]	73.6 [72.8-75.5]	70.3 [70.0-70.6]	68.9 [68.5-69.2]	69.0 [68.6-69.6]
CBFV (cm/s)	21.8 [21.4-23.5]	39.9 [34.7-41.2]	30.9 [22.0-40.0]	26.4 [26.1-27.1]	35.2 [33.5-36.3]	34.7 [33.1-36.1]
Alpha power (%)	0.1 [0.1-0.2]	2.8 [2.0-4.8]	1.7 [0.1-3.0]	0.7 [0.4-1.0]	1.1 [0.5-1.7]	1.0 [0.5-1.6]
Delta power (%)	95.0 [93.8-96.3]	80.2 [70.7-84.9]	87.5 [79.0-94.9]	95.5 [94.3-96.3]	92.6 [90.7-93.9]	92.8 [91.1-94.3]
DAR	923.1 [545.8-1444.8]	29.7 [15.5-42.4]	51.6 [27.0-815.6]	135.8 [98.0-229.8]	85.5 [51.4-174.0]	96.2 [55.8-181.7]

	Patient 3			**Patient 4**		
	OR	*ICU*	*Total*	*OR*	*ICU*	*Total*
TSI (%)	61.7 [61.1-62.1]	61.9 [60.2-64.2]	61.9 [60.2-64.1]	66.8 [65.3-67.5]	69.4 [64.0-69.0]	67.9 [64.3-68.9]
CBFV (cm/s)	43.8 [42.3-45.0]	38.2 [35.9-43.2]	38.5 [35.9-43.8]	26.3 [24.6-28.6]	39.7 [33.1-45.1]	36.5 [32.5-44.7]
Alpha power (%)	0.1 [0.1-0.1]	2.8 [1.9-4.1]	2.6 [1.7-4.0]	2.7 [1.4-10.4]	26.8 [22.8-31.0]	25.9 [21.5-30.4]
Delta power (%)	98.8 [98.4-99.1]	90.5 [87.9-92.9]	90.7 [88.0-93.2]	79.0 [74.5-83.3]	44.1 [36.8-51.3]	45.6 [37.4-54.1]
DAR	1075.1 [714.7-1752.2]	32.8 [21.7-48.8]	34.2 [22.3-53.4]	30.0 [7.4-58.7]	1.6 [1.2-2.2]	1.7 [1.2-2.4]

4.2. Parameters over time

The occurrence of hypoxia and the corresponding supply and demand parameters were plotted over time for all four included patients. Each figure is divided into three subplots. The upper graph shows the averaged TSI. Normoxic TSI is colored blue, while hypoxic TSI is colored red. Baseline TSI and the 10% from decrement are shown in Table 4. The middle graph shows the averaged CBFV. The lower graph shows the relative EEG band powers for the five frequency bands. In each graph, several hours of data is missing, due to one or more data streams being compromised. Note that horizontal axes differ between patients due to the missing data. The plots were fitted to the available data.

Figure 7 shows the selected data for patient 1. All segments show normoxia, indicated a TSI above the 10% decrement line. A gradual increase of theta power and decrease in delta power can be observed after surgery. In the morning after surgery an increase in alpha, beta, and gamma power can be observed compared to the previous day.

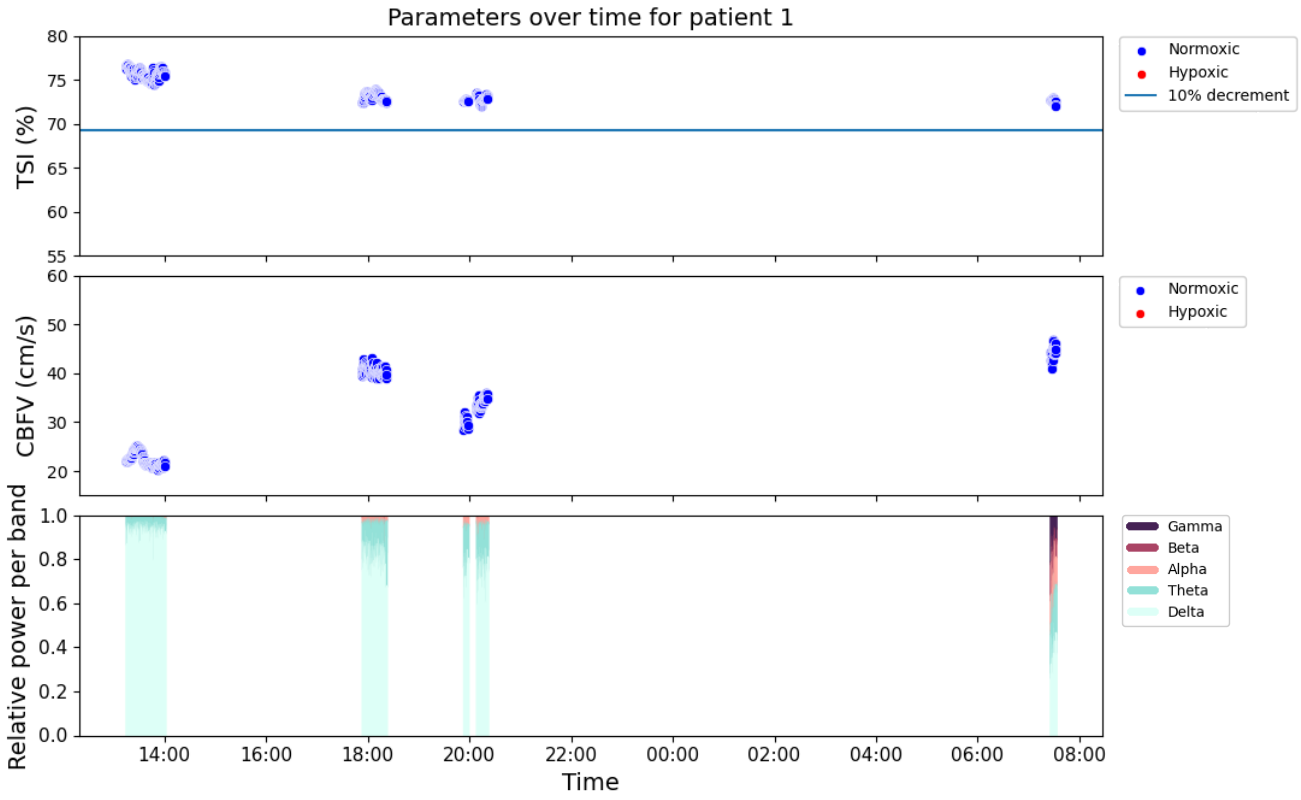

Figure 7: Supply and demand parameters over time for patient 1. The upper graph shows the 30 second averaged Tissue saturation index (TSI). A 10% decrement line from baseline was plotted at 69.3% after baseline was determined to be 77%. All TSI values show normoxia. The middle graph shows the averaged cerebral blood flow velocity (CBFV). The lower graph shows the relative EEG band powers for the five frequency bands. A gradual increase of theta power and decrease in delta power can be observed after surgery. In the morning after surgery an increase in alpha, beta, and gamma power can be observed compared to the previous day. Between 14:00 to 17:53, 18:22 to 19:53 and 20:22 to 07:26 no data was plotted, as one or more data streams was compromised.

Figure 8 shows the parameters over time for patient 2. All segments show normoxia, indicated by the TSI above the 10% decrement line. Around 17:45 a sudden increase in beta and gamma activity can be observed while CBFV and TSI remain stable.

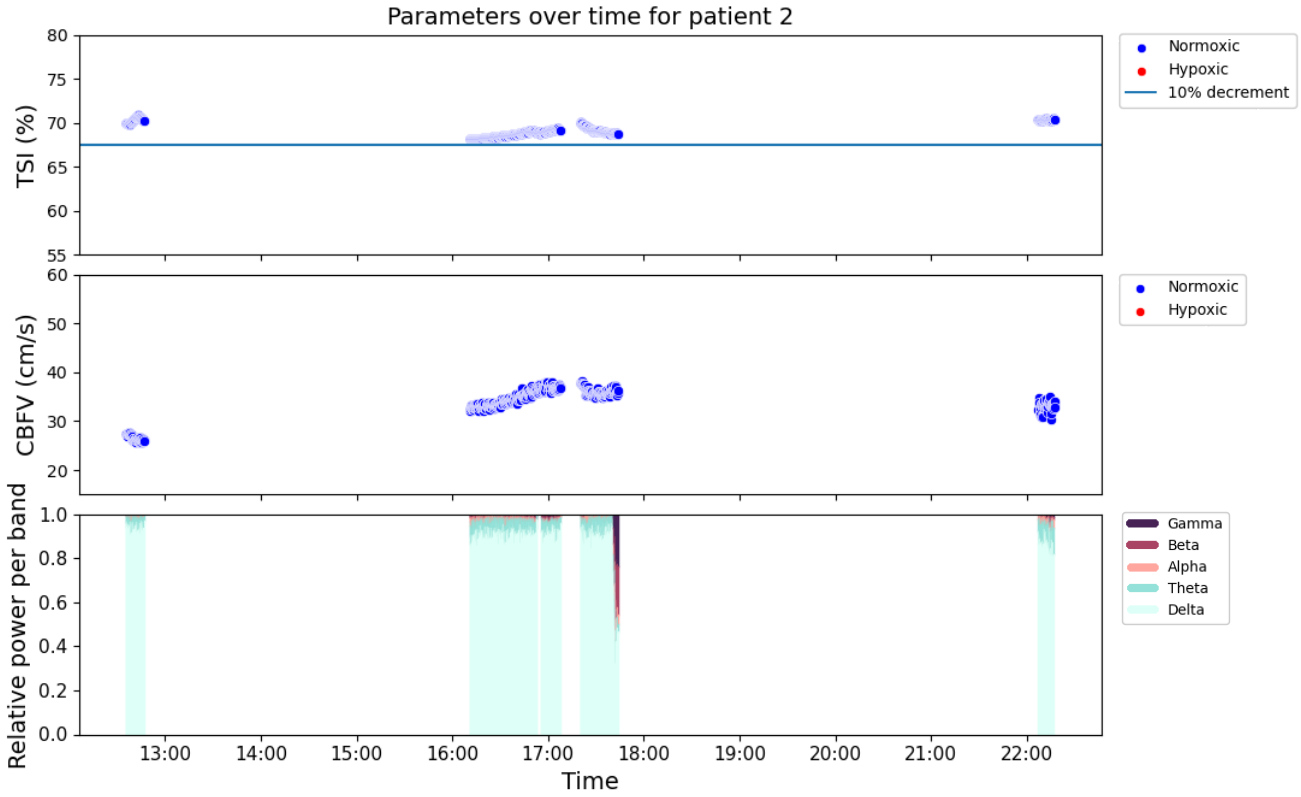

Figure 8: Supply and demand parameters over time for patient 2. The upper graph shows the 30 second averaged Tissue saturation index (TSI). Table 4 shows baseline TSI is 75% and a 10% decrement from baseline is 67.5% for patient 2 and all values exceed this threshold. The middle graph shows the averaged cerebral blood flow velocity (CBFV). The lower graph shows the relative EEG band powers for the five frequency bands. Around 17:45 a sudden increase in beta and gamma activity can be observed while CBFV and TSI remain stable.

Figure 9 shows the parameters over time for patient 3. Patient 3 starts in normoxia but drops to hypoxia around 14:00. After five and a half hours, the first new moment of normoxia is measured around 19:43 after which the patient remains normoxic. Due to the missing data between 14:04 and 16:45 it is not possible to determine whether hypoxia is constant throughout these periods. In this patient, several abrupt changes in CBFV are visible, around 18:20 and 20:30. In the EEG, alpha power varies throughout the measurement.

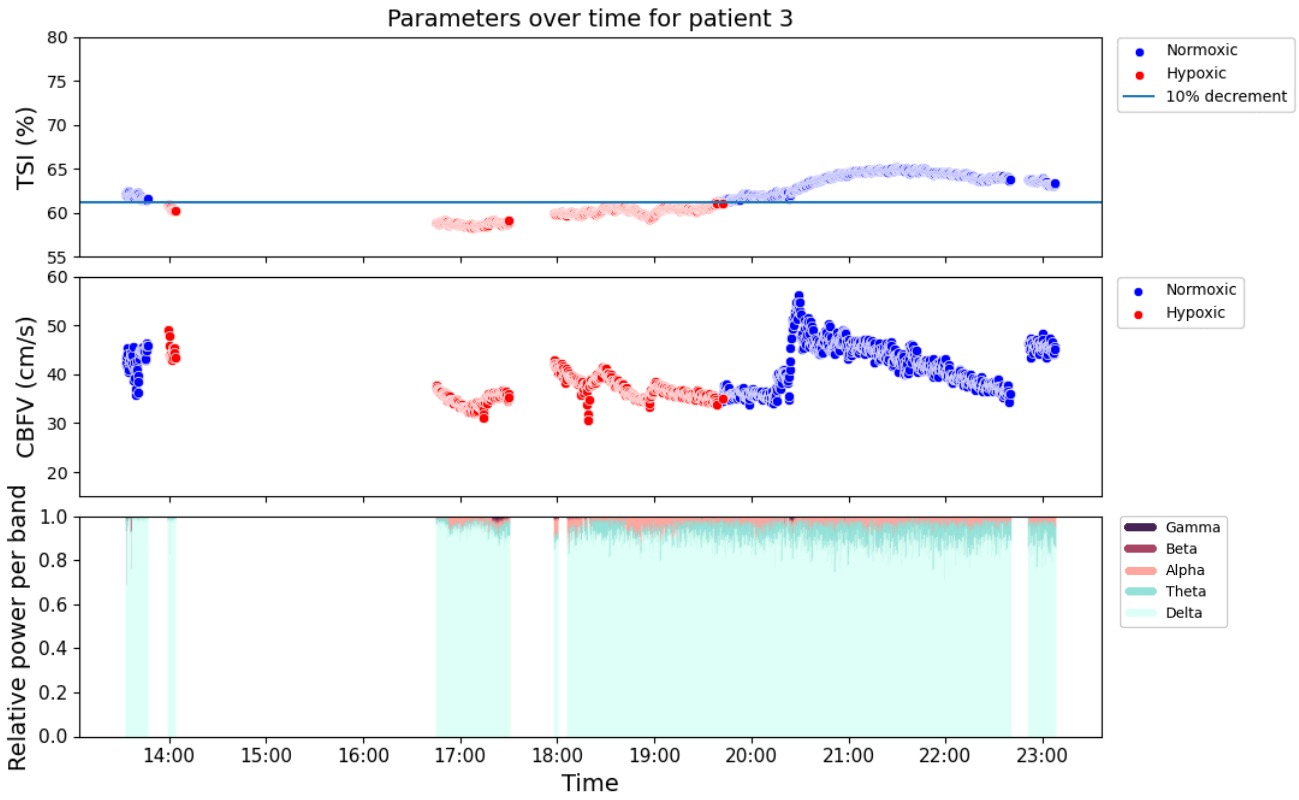

Figure 9: Supply and demand parameters over time for patient 3. The upper graph shows the included 30 second averaged Tissue saturation index (TSI) values. Table 4 shows baseline TSI is 68% and a 10% decrement from baseline is 61.2% for patient 3 and both moments of normoxia and hypoxia can be observed. The middle graph shows the averaged cerebral blood flow velocity (CBFV). Several abrupt changes in CBFV are visible, around 18:20 and 20:30. The lower graph shows the relative EEG band powers for the five frequency bands: delta (0-4Hz), theta (4-8Hz), alpha (8-16Hz), beta (16-32Hz) and gamma (>32Hz). Alpha power varies throughout the measurement.

Figure 10 shows the parameters over time for patient 4. All included segments show hypoxia, indicated by a TSI below the 10% decrement line. Larger amounts of theta and alpha activity can be observed, was well as some beta and gamma activity.

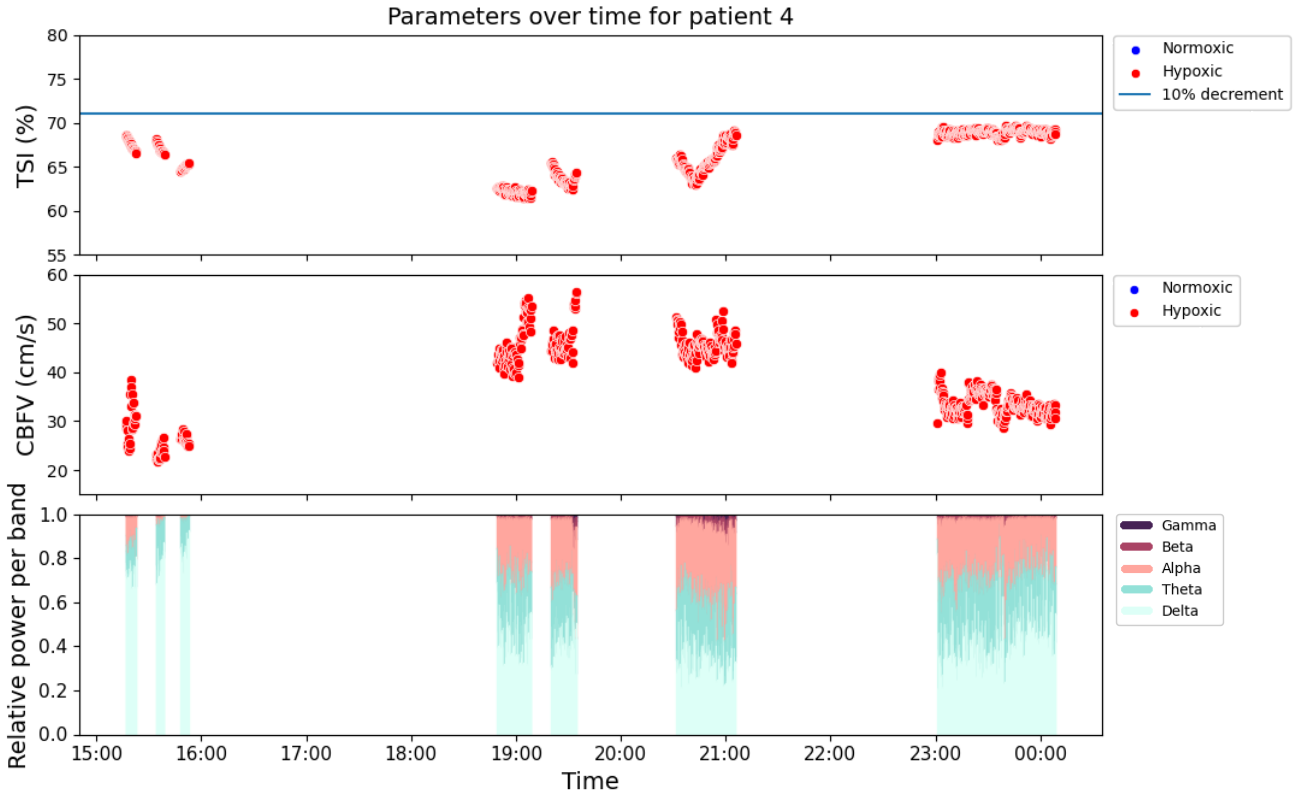

Figure 2: Supply and demand parameters over time for patient 4. The upper graph shows the included 30 second averaged Tissue saturation index (TSI). Table 4 shows baseline TSI is 79% and a 10% decrement from baseline is 71.1% for patient 4 and only hypoxia was measured. The middle graph shows the averaged cerebral blood flow velocity (CBFV). Only moments of hypoxia were measured for patient 4. The lower graph shows the relative EEG band powers for the five frequency bands. Larger amounts of theta and alpha activity can be observed, was well as some beta and gamma activity.

4.3. The NIRS saturation vs jugular venous saturation

To check agreement between regional saturation as measured by the NIRS and the global saturation as measured by the jugular venous oximetry, a scatterplot was constructed (Figure 11). The average TSI within an hour of the blood samples were taken and plotted against $S_{vj}O_2$. Due to limited artifact free data, only 9 jugular venous oximetry measurements between the four patients were included. A significant relationship between TSI and $S_{vj}O_2$ (R^2=0.46, p<0.046) was found. The slope coefficient was 2.05.

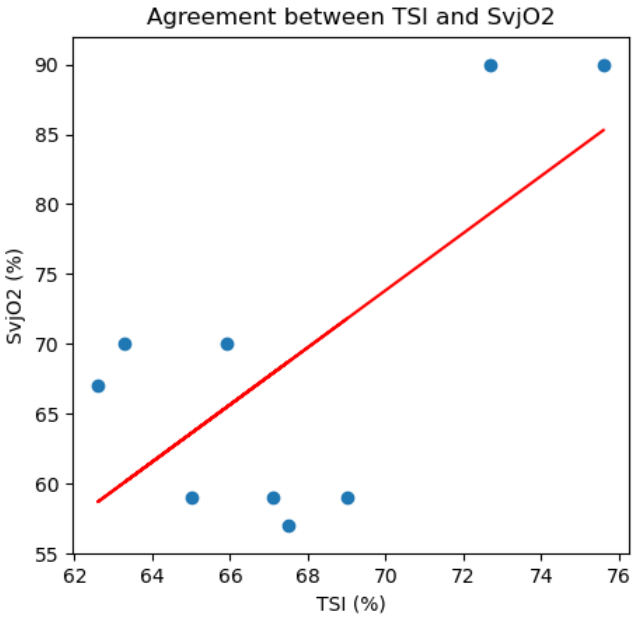

Figure 11: The agreement between tissue saturation index (TSI) and jugular venous oximetry saturation ($S_{vj}O_2$). 9 observations (blue) were plotted, and a regression line was fitted (red).

4.4. Analysis of patient 3

To gain insight into the oxygen balance we analyzed differences in supply and demand between hypoxia and normoxia within patients. Only in patient 3 both moments of normoxia and hypoxia were measured.

4.4.1. Hypoxia

As presented in Table 5, 6 hours, 3 minutes and 30 seconds of artifact free data was gathered, of which 2 hours, 33 minutes and 50 seconds were in hypoxia. After 30-second averaging, 604 hypoxic and 845 normoxic datapoints were included for the primary objective. 130 hypoxic and 37 normoxic datapoints were included for the second objective.

4.4.2. Supply

A histogram was constructed for the difference between the distributions in CBFV for normoxia and hypoxia for patient 3 (Figure 12). The distribution for hypoxia (red) ranges from 31 to 49 cm/s with a peak at 36 cm/s. The distribution for normoxia (blue) ranges from 34 to 56 cm/s with peaks at 36 and 45 cm/s. Distributions were not normally distributed ($p<0.01$). The Kolmogorov-Smirnov statistic was 0.53 ($p<0.01$), indicating that distributions are different. 0.53 is a relatively large value, suggesting that the two distributions are quite different.

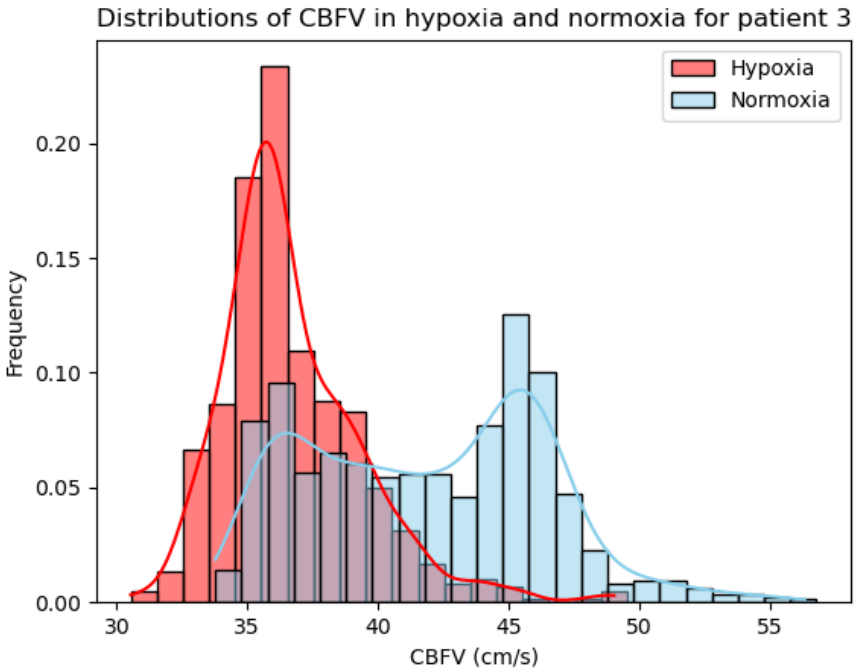

Figure 12: Distributions of cerebral blood flow velocity (CBFV) in hypoxia and normoxia for patient 3. In red, the distribution of CBFV in hypoxia and in blue, the distribution in normoxia. Overlapping values, between 34 and 49 cm/s are colored purple.

To inspect a possible relation between TSI and CBFV, a scatterplot was constructed (Figure 13). The black line at TSI=61.2% represents the threshold for hypoxia. In the low range of TSI (<60%) datapoints are close together and with increase in TSI the spread of datapoints increases. Gaps are visible in the cluster for TSI around 61% between 62.5 and 63.5%. There was a significant relation between TSI and CBFV (R^2=0.43 and p<0.01). The slope coefficient was 1.43.

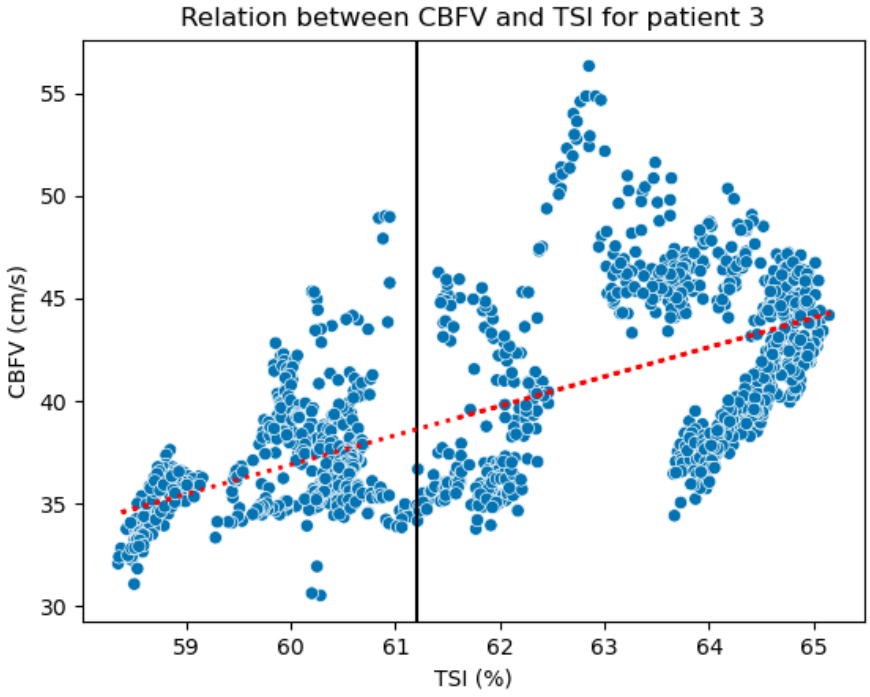

Figure 13: The relation between tissue saturation index (TSI) and cerebral blood flow velocity (CBFV) for patient 3. In blue, datapoint are plotted. The black line shows the threshold for normoxia at TSI=61.2%. In red, the regression line is visible. Datapoints are less spread for low TSI compared to higher TSI.

4.4.3. Demand

A histogram was constructed for the difference between the distributions in relative alpha and delta power for normoxia and hypoxia for patient 3 (Figure 14).

On the left, the distribution for the delta power is shown. The distribution for normoxia (blue) ranges from 70 to 100% with a peak at 89%. The distribution for hypoxia (red) ranges from 80 to 100% with a peak at 87%. Both distributions were not normally distributed ($p<0.01$). The Kolmogorov-Smirnov test showed a Kolmogorov-Smirnov statistic of 0.33 ($p<0.01$), indicating that the distributions differ moderately.

On the right, the distribution for the alpha power is shown. The distribution for hypoxia (red) ranges from 0 to 9% with a peak at 2.2%. The distribution for normoxia (blue) ranges from 0 to 14% with peaks at 2.1%. Both distributions are not normally distributed ($p<0.01$). The Kolmogorov-Smirnov statistic was 0.15 ($p<0.01$), indicating that distributions are significantly different. This is a relatively small value, which suggests that the two distributions differ slightly.

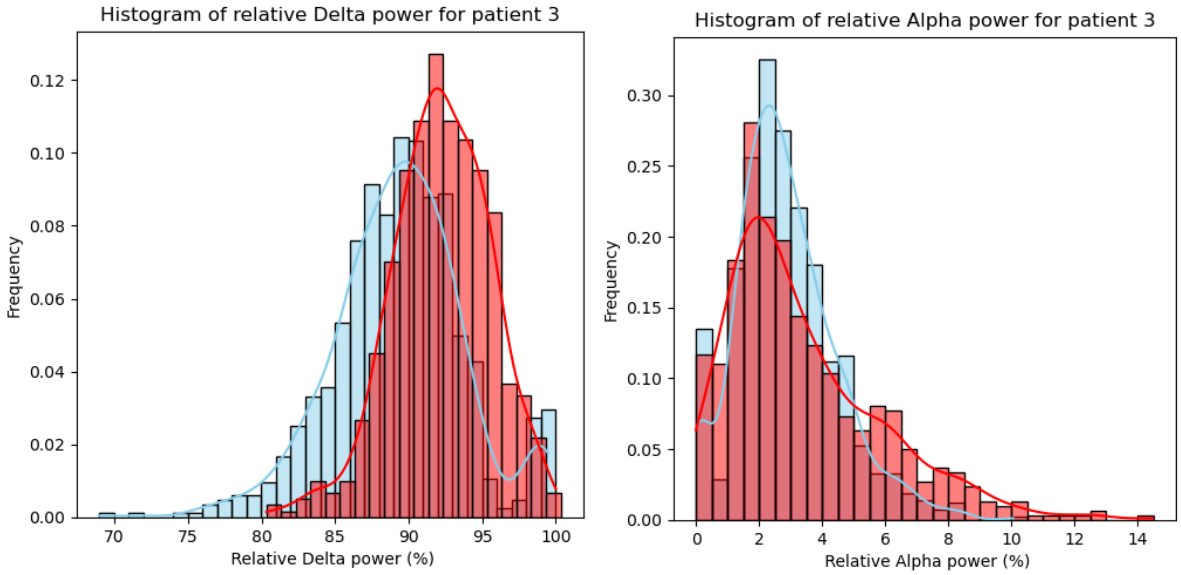

Figure 14: Distributions of delta and alpha power in hypoxia and normoxia for patient 3. On the left, the distribution for delta power in normoxia (blue) ranges from 70 to 100% with a peak at 89%. The distribution for delta power in hypoxia (red) ranges from 80 to 100% with a peak at 87%. On the right, the distribution for the alpha power. The distribution for normoxia (blue) ranges from 0 to 9% with a peak at 2.2%. The distribution for hypoxia (red) ranges from 0 to 14% with peaks at 2.1%.

A histogram was constructed for the difference between the distributions of DAR in normoxia and hypoxia for patient 3 (Figure 15). The distribution for normoxia (blue) ranges from 0 to 1611 with a peak at 34. The distribution for hypoxia (red) ranges from 0 to 1437 with a peak at 33. Both distributions were not normally distributed (Shapiro-Wilk Test=0.22, $p< 0.01$). The Kolmogorov-Smirnov statistic was 0.12 ($p<0.01$), indicating that distributions differ slightly.

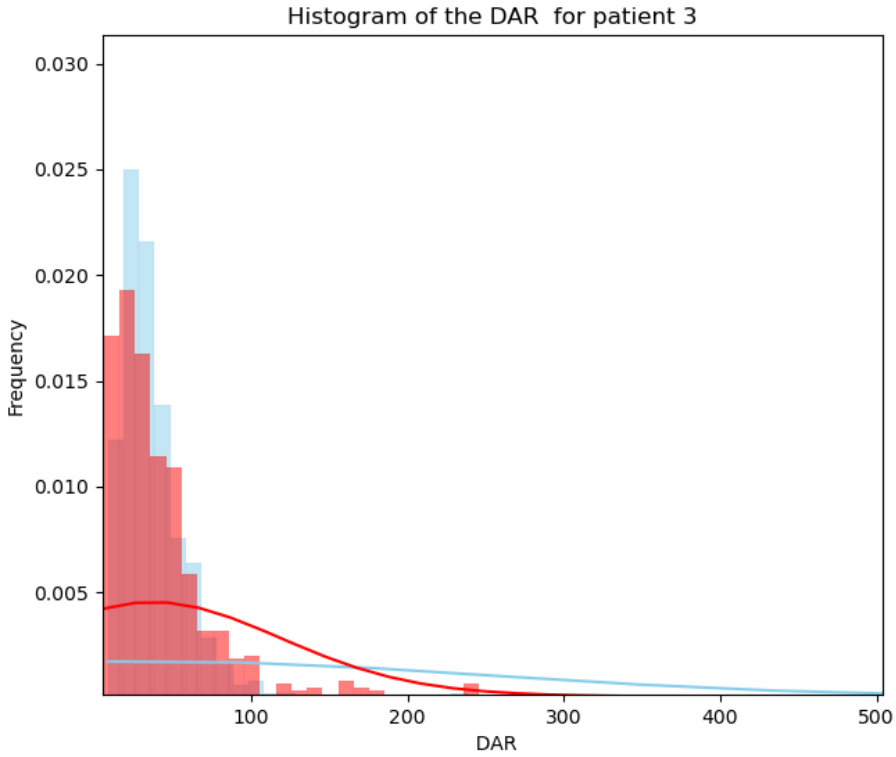

Figure 15: Distributions of delta-to-alpha ratio (DAR) in hypoxia and normoxia for patient 3. In red, the distribution of DAR in hypoxia and in blue, the distribution in normoxia. Overlapping values are colored purple.

4.4.4. Oxygen extraction fraction

The O_2EF_{vj} was calculated to gain insight into the oxygen balance. For patient 3, one jugular venous oximetry measurement falls within an hour of artifact free NIRS data. The blood samples were taken at 20:19 and showed a O_2EF_{vj} of 32.5%. Average TSI was 62.5%

4.4.5. Autoregulation

For insight into the autoregulation, the Mx was calculated and TFA was performed.

4.4.5.1. Mean flow index

A scatterplot was constructed to inspect a possible relation between TSI and Mx, but no relation between the TSI and Mx was found. A histogram was constructed for the difference between the distributions in Mx for normoxia and hypoxia for patient 3 (Figure 16). 27% (35/130) of Mx are greater than 0.45 in hypoxia, 16% (6/37) of Mx in normoxia are greater than 0.45. The distribution for hypoxia (red) ranges from -0.5 to 0.9 with a peak around 0.3. The distribution for normoxia (blue) ranges from -0.3 to 0.5 with a peak around 0.0. Both distributions were normally distributed ($p=0.14$). The Kolmogorov-Smirnov statistic was 0.30 ($p<0.01$), indicating that distributions are different. This is a moderate value, which suggests that the two distributions differ moderately.

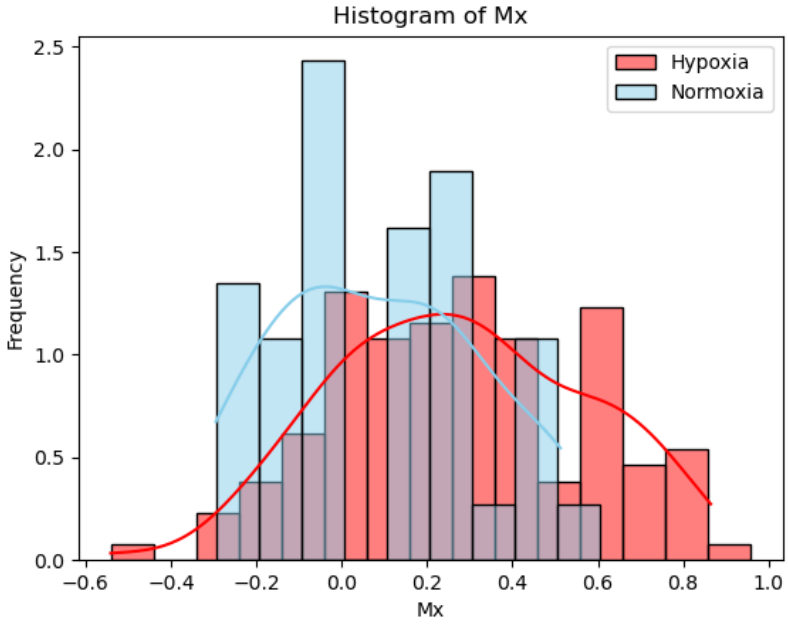

Figure 16: The histogram for the mean flow index (Mx). The distribution for hypoxia (red) ranges from -0.5 to 0.9 with a peak around 0.3. The distribution for normoxia (blue) ranges from -0.3 to 0.5 with a peak around 0.0.

4.4.5.2. Transfer function analysis

After 15-minute averaging, TFA was performed on 30 hypoxic and 3 normoxic windows. Table 8 shows an overview of the outcome parameters phase, gain and coherence from the TFA. Phase is in degrees, gain in $cm*s^{-1}*mmHg^{-1}$ and coherence is dimensionless. Boxplots with the TFA outcomes are presented in Appendix 8.1.

Differences between normoxia and hypoxia are present in the phase, specifically in the LF, HF and total frequency bands. In each of these bands median and IQR are lower in hypoxia. Gain is only different between hypoxia and normoxia for the LF. Here, gain is higher in hypoxia. For the coherence, median and IQR are similar between hypoxia and normoxia for all frequency ranges. After statistical analysis, no significant differences were found.

Table 8: Median values and interquartile ranges of transfer function analysis (TFA) outcomes. Outcomes are reported for the three frequency bands, very-low frequencies (VLF), low frequencies (LF) and high frequencies (HF) and the total frequency range.

	Phase		**Gain**		**Coherence**	
	Normoxia	*Hypoxia*	*Normoxia*	*Hypoxia*	*Normoxia*	*Hypoxia*
VLF	78.2 [78.0-78.9]	64.9 [48.5-87.1]	1.06 [0.93-1.13]	0.98 [0.64-1.30]	0.25 [0.20-0.26]	0.20 [0.09-0.37]
LF	15.15 [-4.56-18.31]	-36.52 [-44.42: -12.21]	1.39 [0.95-1.45]	1.93 [1.55-2.40]	0.40 [0.15-0.44]	0.32 [0.17-0.58]
HF	5.20 [4.78-5.17]	-3.39 [-9.00-1.97]	1.52 [1.03-1.54]	1.43 [1.16-1.70]	0.77 [0.33-0.80]	0.44 [0.29-0.62]
Total	15.02 [10.32-15.67]	-5.75 [-11.74-5.76]	1.46 [0.99-1.47]	1.46 [1.33-1.65]	0.62 [0.27-0.65]	0.44 [0.25-0.54]

4.4.6. Neurovascular coupling

We included 299 hypoxic and 419 normoxic datapoints after averaging. To inspect a possible relation between TSI and the NVC correlation, a scatterplot was constructed. No correlation between TSI and NVC was found.

A histogram was constructed for the difference between the distributions of the NVC correlation for normoxia and hypoxia for patient 3 (Figure 17). The distribution for hypoxia (red) ranges from 0.55 to 1.0 with a peak around 0.99. The distribution for normoxia (blue) ranges from 0.45 to 1.0 with a peak around 0.93. Both distributions were normally distributed ($p<0.1$). The Kolmogorov-Smirnov statistic was 0.50 ($p<0.01$), indicating that distributions are different. This is a relatively large value, which suggests that the two distributions are quite different.

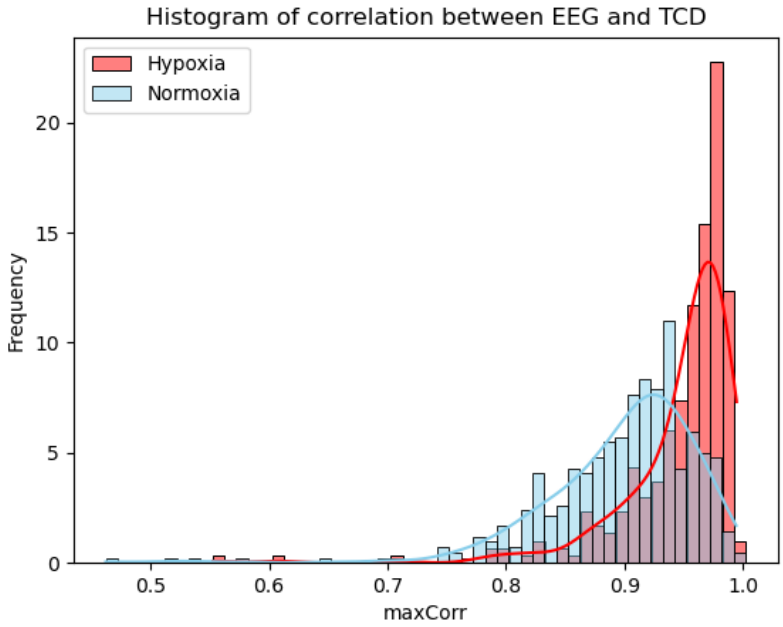

Figure 17: The histogram for maximal correlation (maxCorr) values of the neurovascular coupling (NVC). The distribution for hypoxia (red) ranges from 0.55 to 1.0 with a peak around 0.99. The distribution for normoxia (blue) ranges from 0.45 to 1.0 with a peak around 0.93.

5. Discussion

This study is an extension of a larger pilot study aimed at studying the occurrence and underlying mechanisms of hypoxia following aortic arch surgery through multimodal monitoring. We aimed to study the perioperative occurrence of hypoxia and examine the balance between oxygen consumption and supply during hypoxia.

5.1. Main findings and interpretation

5.1.1. The occurrence of hypoxia

We observed extensive periods of hypoxia in 50% (2/4) of patients. This is of interest, as the occurrence of hypoxia is linked to PND [26], [59].

All hypoxia was classified based on TSI dropping more than 10% from a patient's individual baseline TSI. No TSI below 50% were registered and all values were within the normal ranges found in a healthy population studied by Newman et al. [48]. This study into the normative saturation found a mean baseline TSI of 66% (CI: 51-82%). The inter-individual variations in absolute normal values are high and may be due to variations in pathlength due to skull shape, location of the sensors, photon scattering, skin pigmentation, and the thickness of the skull [60], [61]. Therefore, our findings agree with earlier studies and emphasize the importance patient specific monitoring by comparing TSI to acquired baseline values for determining hypoxia [26], [48], [60].

While this study used a 10% decrement from baseline threshold to classify hypoxia, different cutoffs have been proposed in literature. Studies suggest that 20% or 25% from baseline can be used to effect as well [62], [63], [64]. Subramanian et al. investigated 235 patients, with 50–75% patients presenting with one or more moments of desaturation, which were defined as a decline of 20% or more from baseline [64]. Perioperative desaturation occurred in 63% of high-risk cardiac surgery patient in a study by Dechamps et al., using a 10% threshold [63]. This means that despite differences in exact threshold cutoff, hypoxia based on decrements from baseline are common on the ICU, agreeing with our findings.

A randomized controlled trial using the 10% threshold showed a 97% effectiveness of interventions to reverse hypoxia [63]. These interventions included increasing inspiratory oxygen concentration, normalization of ECC flow, red blood cell transfusion, repositioning the ECC canulae or repositioning the head of the patient. This study highlights the range of available interventions to decrease the occurrence of perioperative hypoxia based on the NIRS signal.

Despite observing hypoxia in two patients, only one developed delirium. This could mean that diagnosing hypoxia through NIRS lacks specificity. This may either be due to the chosen threshold for hypoxia being too sensitive or due to the inherent capability of NIRS to detect hypoxia reliably as NIRS only measures the frontal cortex. A study by Ghincea et al. found only 1 out 3 patients with abnormal NIRS did indeed show signs of stroke [65]. A review by Skrifvars et al. showed the variability reported in rSO_2 signals across different NIRS devices and emphasized the need for standardized cut-offs for preventing hypoxic ischemic brain injury [66].

The fact that only one of the two hypoxic patients developed delirium can also stem from patient-specific physiology. The occurrence of POCD was not included in this study and thus neurological dysfunction might have developed after participation of the study had concluded. After non-cardiac surgery, POCD is found in approximately 26% of patients at 1 week and in 10% to 13% at 3 months following surgery [3]. Furthermore, differences in presence of risk factors could have affected the susceptibility to PND between patients [17], [18]. Finally, hyperperfusion or inflammation were not monitored and might have played a role in the development of PND [19]. As our study was limited by

the number of patients and the limited data per patient, more research into the diagnostic capabilities of NIRS for hypoxia are necessary.

During surgery, regional saturation in the frontal cortex is monitored trough NIRS and detected hypoxia could prompt intervention. The use of NIRS on the ICU, however, is not standard clinical practice and cerebral saturation is no longer monitored. Our study confirms that hypoxia can occur on the ICU, while the patient is monitored less closely. Monitoring of cerebral saturation compared to a baseline saturation at the ICU could allow for patient specific interventions, which may prevent or limit the occurrence of and damage from hypoxia.

5.1.2. The oxygen balance for patient 3

Since both normoxia and hypoxia were observed exclusively in patient 3, further analyses on supply and demand were only performed on this patient.

5.1.2.1. Hypoxia

Our results show that the patient was hypoxic for at least 2 hours and 33 minutes. The extent of neurological damage from hypoxia is influenced by its duration and severity [67]. Despite not knowing the total duration of hypoxia, these hours were significant as neurological damage can occur after only minutes of hypoxia [33], [35], [68]. Therefore, it's plausible that the observed hypoxia has played a role in the development of PND in this patient. While the duration of the hypoxia was extensive, the severity was difficult to quantify using NIRS, as NIRS only measures locally. More frequent measurements with jugular venous oximetry could provide further insight into the severity of the hypoxia. This is important because a moderate desaturation can prompt loss of function but still allow the neurons to survive, while a more severe desaturation would cause ischemia [68].

Figure 9 and table 5 show the extent of the missing data. Data was missing between three intervals of hypoxia, around 14:15, 17:00, and 18:00. It was not known whether hypoxia persisted during these segments. Additionally, from 22:07 onwards no data was included. The large amounts of missing data made it impossible to get a clear picture of the full duration and severity of the hypoxia. A more complete dataset is required before defining the duration and severity of hypoxia [68].

5.1.2.2. Supply

While the distributions of CBFV between hypoxia and normoxia differed significantly, the distributions overlap. While a low CBFV does not guarantee hypoxia, our results suggest that a higher CBFV (>42 cm/s) has a high likelihood of the patient being normoxic. Striving for a higher CBFV might have a protective effect, but further research is needed to confirm this on a larger population.

Patient 3 showed a positive correlation between TSI and CBFV and this correlation is to be expected. The oxygen content of cerebral venous blood represents the matching of cerebral blood flow (CBF) to the cerebral metabolic rate of oxygen. As 70-80% of the cerebral tissue consists of venous compartment, the TSI is heavily dependent the venous oxygenation [69]. When assuming a constant oxygen consumption, a higher inflow of oxygenated blood will increase the cerebral venous oxygen content and increase the saturation. A study by Holzshuh et al. found a positive correlation between CBFV and O_2Hb changes [69]. The researchers measured CBFV and O_2Hb before and after administering acetazolamide, which actively increases CBF. While TSI and O_2Hb are not the same outcome parameter, they are closely linked because TSI is calculated from the O_2Hb as shown in equation 1. Furthermore, a study by Moritz et al. found that NIRS and TCD measurements provided similar accuracy for the detection of cerebral ischemia during carotid surgery [70] While surgical circumstances were different to aortic arch surgery, both TCD and NIRS showed good sensitivity and

specificity for detecting ischemia. The studies further demonstrated the likelihood of TCD and NIRS being indeed correlated, agreeing with our findings.

The variance of the scatterplot increased with increasing TSI. This indicates that a higher TSI related to a more variable CBFV. From a physiological point of view, this increased variation can be explained by effects from the cerebral autoregulation. When saturation is sufficient and ABP is within limits, the autoregulation regulates the CBFV to maintain sufficient saturation [38]. We hypothesize that when CBFV is too low and the brain becomes hypoxic, the autoregulation is incapable of lowering the vascular resistance further and the saturation becomes more correlated with the CBFV. This idea fits with the hypothesis that cerebral control mechanisms adapt and can lower CBFV despite sufficient saturation. However, the increased variance is not recognized by Holzshuh et al. and is not further discussed in literature. It is also possible that the increased variance is simply due to inaccurate measurements. TCD requires technical skill and is highly susceptible to variations in insonation angle [71], [72]. Therefore, slight deviations might have caused significant changes in measured CBFV.

5.1.2.3. Demand

The DAR was calculated as experimental measure to quantify cerebral activity. Despite the statistical difference in hypoxic and normoxic distributions, the distributions overlapped greatly. No difference between normoxia and hypoxia could be made based on the DAR, due to this overlap.

Despite the DAR being described for use in detection of ischemia in the ICU, we saw very high DAR values (>20), which didn't occur in other studies [33], [34] A study by Finnigan et al. found a median DAR of 4.27 (range 1.38-14.15) in patients with a sub-acute ischemic stroke. Another study by Finnigan et al. demonstrated high sensitivity and specificity to acute ischemia, while finding maximum DAR values of 14 [33].

Our high DAR values can be explained by the minimal amount of alpha power during and after surgery. It is possible that our patients were more deeply sedated and cooled during and after surgery compared to other studies researching the DAR. Depth of anesthesia, medications, hypothermia, and pre-existing cortical injury all are confounding factors that limit the sensitivity of EEG for detecting cerebral ischemia [35]. Because the absent alpha power strongly affects the DAR, the DAR appears to be a less suitable measure for this patient group.

An alternative for the DAR might be the median frequency of the EEG [73]. This measure can be used to determine depth of anesthesia and is not affected using specific frequency bands. Therefore, when alpha and delta powers are out of balance, the median frequency does not produce extreme values in contrast to the DAR. Additionally, the influence of the theta and gamma bands are included in the measure, giving a more comprehensive overview.

Despite the lack of information from the DAR, the alpha and delta band powers themselves gave some insight into differences between normoxia and hypoxia. Figure 14 and table 7 show higher delta power, slightly lower theta power, and equal alpha power in hypoxia compared to normoxia and suggesting lowered brain activity during hypoxia. Lower cerebral activity can be explained both by lower oxygen demand and the presence of hypoxia. Due to missing pieces of data, it was not possible to ascertain whether EEG decreased after insufficient supply of oxygen or vice versa. The presence of hypoxia suggests oxygen deprivation, appropriate to the lower flow velocity in hypoxia.

The comparison between hypoxia and normoxia did not account for the passage of time. Almost all the moments of hypoxia fell before the moments of normoxia. This may have had a possible effect because after surgery on the ICU, anesthesia was diminished, cooling was stopped, and thus the brain became more active. Thus, it is possible that the increase in activity between hypoxia and normoxia

could have been affected by these confounders. Although we were aware of the importance of time in approaching the problem, we did not manage to find a suitable approach.

While the quantitative EEG provided useful insight into the cerebral activity, drawing conclusions regarding the oxygen demand is difficult, as slowing of the EEG can be normal or pathological, differences were small and confounding factors were present [74]. Again, depth of anesthesia, medications, hypothermia, and pre-existing cortical injury are confounding factors limiting the sensitivity of EEG for detecting ischemia [35]. Before clinical use is possible, research should focus on establishing normal trends for cerebral activity after surgery. If these trends are known, deviations from these trends could warn interventions to prevent PND.

5.1.2.4. Oxygen extraction fraction

For patient 3, only one jugular venous oximetry measurement out of the four successful measurements fell within an hour of available NIRS data. The O_2EF_{vj} of 32.5% was registered during normoxia. This value falls within ranges found by a study in healthy participants by Jiang et al., suggesting that the patient had a normal oxygen extraction during normoxia [75]. As we only obtained one relevant measurement, the difference between hypoxia and normoxia could not be compared. In future research, ensuring artifact free data streams before taking a blood sample is necessary for linking the jugular venous oximetry measurements to the other parameters.

5.1.2.5. Cerebral autoregulation

The secondary objective was to investigate whether disturbed autoregulation or neurovascular coupling may have influenced cerebral perfusion during hypoxia. The histogram of the Mx (Figure 16) suggests that moments of impairment of the autoregulation were present both in normoxia and hypoxia. Notably, Mx values greater than 0.45 were present more often and much higher (>0.7) in hypoxia, compared to normoxia. This is highlighted by the hypoxic distribution being closer to 1.0. While a threshold of 0.45 was used for determining whether autoregulation was active or impaired, there were differences in severity of impairment [55]. A Mx of 0.5 and 1.0 both suggested impairments, but a Mx of 0.5 suggests that the autoregulation still functions, albeit partially. The higher Mx levels (>0.7) in hypoxia suggest that there are moments of severe autoregulation impairment in hypoxia. While a low Mx does not rule out hypoxia, our results suggest that a higher Mx has a higher likelihood of the patient being hypoxic.

In this study the threshold of Mx of 0.45 was used to define impaired cerebral autoregulation [55]. This threshold is a topic for discussion, as studies have also reported impaired cerebral autoregulation by using a threshold of 0.3 [76], [77]. We chose the threshold to match methodology by Brady et al. [54].

The Mx could be influenced by the rate at which ABP changes. The dynamic autoregulation is more capable of adapting to slow ABP changes compared to quick changes [38]. When comparing two patients with equally optimal autoregulation, the patient with more rapidly changing blood pressure will show a higher Mx. The rate of change in ABP was not accounted for in the Mx. Because the rate of ABP change was not included in the calculation it was possible that values of the Mx are affected. We believe that this is an inerrant limitation of the Mx. While this limitation may have affected our results, we do not expect significant differences in ABP change between the normoxic and hypoxic segments.

The passage of time may have affected the results. Patient 3 first showed a long period of hypoxia before normoxia reappeared. Given the effect of hypoxia over time, it may be that autoregulation is still recovering from the hypoxic period and during normoxia, showing higher Mx. Moreover, it is possible that the cerebral vasculature is still recovering from surgery and therefore showed a higher Mx.

Patient 3 is known to have developed PND and shows high Mx during hypoxia indicating severely impaired autoregulation. While this study does not compare Mx between patients, our found impairment combined with the occurrence of PND suggests impaired autoregulation may have played a role in developing PND. A study by Crippa et al. showed cerebral autoregulation was altered in half of the patients with sepsis and was associated with the development of brain dysfunction [77]. Future research should focus on defining a reliable threshold for impaired autoregulation, which could be implemented for clinical interventions.

In addition to calculating the Mx, TFA was performed. TFA provided more information compared to the Mx but was more complex in its interpretation. The cerebral autoregulation will be discussed through the phase, gain, and coherence between the ABP and CBFV.

A phase approximating 0 indicates 1-to-1 transmission of ABP waves and thus worsened autoregulation compared to a higher phase. In hypoxia, a phase around 0 was visible in the HF and total frequency ranges. In normoxia, phases around 0 were also visible in the LF and HF ranges. We could not conclude that autoregulation was altered in hypoxia based on the phase, as no significant differences could be found between normoxia and hypoxia. The phases in the VLF range were significantly higher compared to the other frequency bands. Compared to reference values from Meel-van den Abeelen et al., the phases in this study were higher in the VLF range, lower in the LF range and similar in the HF range [42], [43]. This might indicate that the autoregulation of patient 3 was capable of dampening very low frequency changes in ABP but was incapable of adapting to the low and high frequencies.

A high gain indicates a poor autoregulation [78], as it means that changes in ABP cause strong CBFV changes. When comparing hypoxia and normoxia in table 8 and the boxplots in appendix 8.1, we see a higher gain in hypoxia in the LF and total frequency range and a similar gain in the VLF and HF frequency range. The highest values of the gain of each frequency band occur in hypoxia. Compared with reference values from Meel-van den Abeelen et al., the gains found in this study were increased in all frequency bands, both in normoxia and hypoxia [42], [43]. This indicates that our patient may have had an impaired autoregulation throughout our measurements compared to a healthy population. All our included data was measured postoperatively, and the impaired autoregulation may be due to impact from the surgery.

High coherence indicates a linear relation between ABP and CBFV [78]. A linear relation can indicate impaired autoregulation but is also affected by the speed at which ABP changes because autoregulation is less able to accommodate rapid pressure changes. In the VLF and LF ranges during hypoxia some coherence values were increased compared to normoxia, indicating a worsened autoregulation. Compared to normal values, coherence values in our study were relatively low. Lower coherence indicates that there is no linear correlation, which could be caused by activated autoregulation, but also by the presence of noise [42], [43]. During data selection we excluded noisy data and the likelihood of influence is therefore small. The low coherence indicates a that the autoregulation is present.

In summary, the comparison with reference values showed an increased gain in hypoxia and normoxia, indicating suboptimal autoregulation. It is possible that after surgery and after a period of hypoxia, the autoregulation was still recovering during the moments of normoxia. It was thus questionable to what extent the autoregulation in normoxic segments were truly "healthy". Simultaneously, the coherence suggests autoregulation is present. It is difficult to draw a definitive conclusion from the TFA as results were contradictory between frequency bands.

The comparison between normoxia and hypoxia was possibly affected by the quantity of data. There were only 5 segments in normoxia. Figures 19, 20, and 21 show very low variance in the normoxic data

points. An 80% window overlap was used in the method. With that, the low spread of the normoxia may have been influenced by overlap in the data segments, making variance appear smaller.

The inconsistency in outcomes and the complexity of interpretation mean that TFA is not yet ready for use at the bedside. In addition to more data from a greater population, a more concrete threshold for impaired autoregulation is needed.

5.1.2.6. Neurovascular coupling

An experimental measure for estimating the NVC has been introduced. Calculation of the maximal cross correlation between the DAR and the CBFV was performed, because with intact NVC cerebral activity and cerebral blood flow should be correlated. The ranges of the distributions were nearly equal, but the median of the hypoxic distribution was closer to 1.0 compared to normoxia. We expected to find a stronger correlation in the normoxic segments.

An explanation for this unexpected finding is that the strength of the correlation might have been affected by the rate at which DAR and CBFV increased. As the DAR is a ratio, a linear decrease of alpha power results in a hyperbolic increase in DAR. The linearly increasing CBFV was changing at a linear rate, while the hyperbolically increasing DAR was increasing at an accelerating rate. So, even though they were both increasing, they were not moving together in a linear fashion, which decreased the strength of correlation.

Current research into the optimal method of NVC is ongoing. Different combinations of techniques, including TCD, NIRS, EEG and MRI have been studied. We implemented the new approach without first having implemented previously researched methods due to time constraints. We suggest future researchers focus on validating existing and more promising methods of determining NVC.

5.1.2.7. Overview of discussed points

Moments of hypoxia were present during surgery, and afterwards on the ICU. During hypoxia, there was a lowered CBFV and slightly lowered cerebral activity. Additionally, higher values of impaired autoregulation were found in hypoxia through the Mx. The TFA and correlation for the NVC yielded inconclusive results. Our findings are in accordance with the hypothesis that there is disbalance of supply and demand of oxygen during hypoxia. However, due to the amounts of missing data, it was impossible to know the full duration and severity of the hypoxia. Ensuring proper oxygen balance could prevent the hypoxia and reduce risk of PND and monitoring of hypoxia is an important step in prevention. However, differences between normal and hypoxic parameters were small and distributions overlap making clinical interpretation difficult.

5.1.3. The NIRS versus the jugular venous oximetry

NIRS data and jugular venous oximetry samples were compared to check for agreement and a positive correlation between TSI and $S_{vj}O_2$ was observed.

A positive correlation was anticipated because a lowered regional saturation can correspond to a lowered global saturation if the cause of the decrease has global effect. While this relation was anticipated, the anatomic regions that each technique measures should be considered. The NIRS monitored the saturation in a small but important cerebral region, as it monitored most distal region supplied by the MCA and the ACA [26]. We expected that in the case of global hypoperfusion, this region would desaturate first. Therefore, we expected that NIRS could detect hypoxia at an early stage and, correspondingly, had a higher sensitivity for detecting hypoxia compared to the jugular venous oximetry. Furthermore, as NIRS measured regionally and the jugular venous oximetry measured globally, local events, such as a stroke, could affect the measures unequally, depending on the severity and location of the event.

The positive correlation between TSI and $S_{vj}O_2$ was weak due to the few data points. A study by Naguib et al. showed that stronger correlations (R>0.59) with larger sample sizes are possible [79]. Beside the low number of data points, several factors may have influenced the correlation. In our study, the 60-minute averaged TSI was compared to each jugular venous oximetry measurement. Our graphs showing TSI over time illustrated that TSI can vary significantly within an hour and variations in TSI might have influenced the correlation with the $S_{vj}O_2$. Furthermore, Cindel Albers described in her thesis that jugular venous oximetry measurements were possibly affected by incorrect aspiration during sampling leading to measurement errors. Finally, studies have shown that NIRS measurements can be influenced by extracerebral tissue [80]. ABP can influence perfusion of extracerebral tissue, leading to different TSI levels, regardless of cerebral saturation. It is possible that in our results TSI was also influenced by altered perfusion of extracerebral tissue. A greater number of datapoints from a larger population is needed before conclusions on the agreement can be drawn. Furthermore, correct aspirations of the blood samples are necessary for reliable jugular venous oximetry results.

5.2. Limitations and recommendations

5.2.1. Recording efficiency

Gathering synchronized and artifact free data with NIRS, TCD and EEG simultaneously has proven to be a challenge. Only 15.1% of recording time yielded usable data, making it impossible to completely understand the duration and severity of hypoxia. Moreover, we were unable to follow trends into the oxygen balance over time. Three causes contributed to the limited data availability: the presence of artifacts, the desynchronization of data, and the choice of data selection.

5.2.1.1. Presence of artifacts

Two main types of artifacts were of concern: shorter movement artifacts and displacement artifacts.

Shorter movement artifacts were present in NIRS, TCD, ABP and EEG data as short bursts of noise, after which the physiological signal would be restored. These artifacts were prevalent but were of limited concern, as signals would return after the artifacts. Additionally, data could be repaired by linear interpolation if artifacts were shorter than three heartbeats.

Displacements of the NIRS, TCD, EEG resulted in artifacts which could not be restored. The TCD was most prone to displacement. Small adjustments to the probes, e.g. from movement of the patient, lead to significant changes in signal quality and/or CBFV value. Differences in registered CBFV due to differences in insonation angles were measurement errors and could not be recovered by postprocessing of the data. Larger adjustments to the probes caused the signal to disappear completely. This is an inherent limitation of the TCD. Displacement of the probes was only checked intermittently, so displacements had a long-lasting effect. Displacement of EEG electrodes occurred sparsely and was of little influence on the included data. Displacement of NIRS optodes occurred mainly at the start of the night which led to missing data until the next morning.

While movement artifacts are unavoidable, the effect of displacement of devices can be kept to a minimum by regular checks. Future studies should try to obtain at least 30-minute periods of consecutive clean data with all modalities. This should give the opportunity to get an overview of the oxygen balance and allow for more complex data analysis such as TFA. Taking blood samples for jugular venous oximetry measurement can be done halfway during an epoch so that samples are relevant for the data. The 30-minutes periods should be taken as often as possible to gain insight into progression over time. This may be challenging in practice due to logistical reasons.

5.2.1.2. Desynchronization

The occurrence of data gaps resulted in desynchronization of the data from the bedside monitor. As properly synchronized data was crucial for obtaining reliable results, insufficiently synchronized data had to be excluded. Sufficient synchronization was not possible by the algorithm of the UMCG in two out of eight datafiles. As discussed in chapter 2, the cause of the problem has been resolved. In future research with the setup, less data will likely have to be excluded.

Moreover, desynchronization of NIRS data between the Oxysoft and ICM+ datasets was observed. While relevant time shifts were compensated for, the shifts showed the fragility of the current setup. In our setup, the NIRS data is only imported into ICM+ as averaged data over time, instead of raw waveform data. Importing waveform data into ICM+ and saving waveform data in Oxysoft would allow for more accurate comparison between datasets and would allow for more accurate synchronization when necessary.

To further improve accurate synchronization of data, future researchers could improve the monitoring setup. TCD was not saved as raw data and only imported into ICM+. DWL, the recording software for TCD, has the option to save the CBFV waveforms to text files. By saving CBFV as raw files in addition to the streaming the waveforms, data will not be lost if the ICM+ program fails. Saving the TCD and NIRS data both as waveform data in ICM+ and as separate files in their respective recording software should function as a redundancy step. This redundancy step only works for problems within ICM+ and problems stemming from within DWL or from inadequate data collection are not helped.

5.2.1.3. Approach to data selection and analysis

The nature of the research question meant that only when NIRS, TCD, and EEG all provided clean data, analyses could be performed to answer the research question. This meant that if one of the modalities failed, the data of the other two would be discarded. This step was necessary, as including data with two out of three techniques would have introduced bias. Despite the necessity, a lot of data had to be discarded due to this approach and this compromised the possibilities to study the trends thoroughly.

Furthermore, visual inspection was used for the selection of artifact free data. Visual inspection is inherently subjective, as it relies on the individual's interpretation of the data [81]. Factors such as fatigue, distractions, or lack of training can affect the performance of the inspector. Combined, this can lead to inconsistencies and biases in the data selection process. Despite its drawbacks, visual inspection was used due to the many different types of artifacts and the need for high data quality. To mitigate the risks, artifact detection algorithms might assist in the selection process. While each algorithm comes with its own advantages and disadvantages, use of a validated algorithm might help reduce inconsistencies.

5.2.2. Number of included patients

The inclusion of only four patients, of which one was suitable for our research question, limited the generalizability and the ability to draw conclusions with certainty. The four patients included in our study were of different ages, surgical approaches, and outcomes. NIRS and TCD measurements and EEG signals are prone to inter-patient variability. These factors are of interest because the etiology of PND is believed to be multifactorial. It is likely that our measures will differ between patients and the generalizability of our results is limited. A larger sample size would improve reliability and allow for more comprehensive analyses. Future studies with larger and more diverse patient cohorts are required to validate our findings and address these limitations.

6. Conclusion

This study aimed to study the perioperative occurrence of hypoxia and examine the balance between oxygen supply and demand during hypoxia. Our results showed that hypoxia can occur postoperatively. Monitoring saturation deviations from baseline on the ICU could prompt interventions to prevent hypoxia and reduce risk of PND. Definitive conclusions on oxygen balance could not be drawn due to the amount of missing data and low number of included patients. However, the lowered cerebral flow and cerebral activity in hypoxia suggest an oxygen imbalance. Future studies should try to obtain consecutive clean data with all modalities simultaneously, so that oxygen balance can be assessed more accurately.

7. References

[1] J. Z. Qu *et al.*, "Brain Protection in Aortic Arch Surgery: An Evolving Field," *J Cardiothorac Vasc Anesth*, vol. 35, no. 4, pp. 1176–1188, Apr. 2021, doi: 10.1053/j.jvca.2020.11.035.

[2] B. Milne, T. Gilbey, L. Gautel, and G. Kunst, "Neuromonitoring and Neurocognitive Outcomes in Cardiac Surgery: A Narrative Review," *J Cardiothorac Vasc Anesth*, vol. 36, no. 7, pp. 2098–2113, Jul. 2022, doi: 10.1053/j.jvca.2021.07.029.

[3] R. Hood, A. Budd, F. A. Sorond, and C. W. Hogue, "Peri-operative neurological complications," *Anaesthesia*, vol. 73, pp. 67–75, Jan. 2018, doi: 10.1111/anae.14142.

[4] J. Liu *et al.*, "Incidence, Predictors and Outcomes of Delirium in Complicated Type B Aortic Dissection Patients After Thoracic Endovascular Aortic Repair," *Clin Interv Aging*, vol. Volume 16, pp. 1581–1589, Aug. 2021, doi: 10.2147/CIA.S328657.

[5] S. J. Aitken, F. M. Blyth, and V. Naganathan, "Incidence, prognostic factors and impact of postoperative delirium after major vascular surgery: A meta-analysis and systematic review," *Vascular Medicine*, vol. 22, no. 5, pp. 387–397, Oct. 2017, doi: 10.1177/1358863X17721639.

[6] C. W. Hogue, C. A. Palin, and J. E. Arrowsmith, "Cardiopulmonary Bypass Management and Neurologic Outcomes: An Evidence-Based Appraisal of Current Practices," *Anesth Analg*, vol. 103, no. 1, pp. 21–37, Jul. 2006, doi: 10.1213/01.ANE.0000220035.82989.79.

[7] D. H. Tian *et al.*, "A meta-analysis of deep hypothermic circulatory arrest versus moderate hypothermic circulatory arrest with selective antegrade cerebral perfusion," *Ann Cardiothorac Surg*, vol. 2, no. 2, p. 148, 2013.

[8] K. I. de la Cruz, J. S. Coselli, and S. A. LeMaire, "Open aortic arch replacement: a technical odyssey," *J Extra Corpor Technol*, vol. 44, no. 1, p. P42, 2012.

[9] C.-H. Chen *et al.*, "Acute infarcts on brain MRI following aortic arch repair with circulatory arrest: insights from the ACE CardioLink-3 randomized trial," *Stroke*, vol. 54, no. 1, pp. 67–77, 2023.

[10] T. Berger *et al.*, "Risk factors for stroke after total aortic arch replacement using the frozen elephant trunk technique," *Interact Cardiovasc Thorac Surg*, vol. 34, no. 5, pp. 865–871, 2022.

[11] S. Otomo, K. Maekawa, T. Baba, T. Goto, and T. Yamamoto, "Evaluation of the risk factors for neurological and neurocognitive impairment after selective cerebral perfusion in thoracic aortic surgery," *J Anesth*, vol. 34, pp. 527–536, 2020.

[12] O. Preventza *et al.*, "Neurologic complications after the frozen elephant trunk procedure: a meta-analysis of more than 3000 patients," *J Thorac Cardiovasc Surg*, vol. 160, no. 1, pp. 20–33, 2020.

[13] S. Cai *et al.*, "Prevalence, predictors, and early outcomes of post-operative delirium in patients with type A aortic dissection during intensive care unit stay," *Front Med (Lausanne)*, vol. 7, p. 572581, 2020.

[14] Z. Liu, X. Pang, X. Zhang, G. Cao, C. Fang, and S. Wu, "Incidence and Risk Factors of Delirium in Patients After Type-A Aortic Dissection Surgery," *J Cardiothorac Vasc Anesth*, vol. 31, no. 6, pp. 1996–1999, Dec. 2017, doi: 10.1053/j.jvca.2016.11.011.

[15] M. Fang *et al.*, “Risk Factors and Prediction of Postoperative Delirium in Aortic Arch Replacement: A Retrospective Cohort Study,” *Journal of Translational Critical Care Medicine*, vol. 5, no. 1, p. e00004, 2023.

[16] A. Dubovoy *et al.*, “Forbidden word entropy of cerebral oximetric values predicts postoperative neurocognitive decline in patients undergoing aortic arch surgery under deep hypothermic circulatory arrest,” *Ann Card Anaesth*, vol. 20, no. 2, pp. 135–140, 2017.

[17] Y. Carrascal and A. L. Guerrero, “Neurological Damage Related to Cardiac Surgery,” *Neurologist*, vol. 16, no. 3, pp. 152–164, May 2010, doi: 10.1097/NRL.0b013e3181bd602b.

[18] K. J. Schenning and S. G. Deiner, “Postoperative Delirium in the Geriatric Patient,” *Anesthesiol Clin*, vol. 33, no. 3, pp. 505–516, Sep. 2015, doi: 10.1016/j.anclin.2015.05.007.

[19] J. R. Maldonado, “Neuropathogenesis of Delirium: Review of Current Etiologic Theories and Common Pathways,” *The American Journal of Geriatric Psychiatry*, vol. 21, no. 12, pp. 1190–1222, Dec. 2013, doi: 10.1016/j.jagp.2013.09.005.

[20] D. R. Skvarc *et al.*, “Post-Operative Cognitive Dysfunction: An exploration of the inflammatory hypothesis and novel therapies,” *Neurosci Biobehav Rev*, vol. 84, pp. 116–133, Jan. 2018, doi: 10.1016/j.neubiorev.2017.11.011.

[21] F. Scholkmann, A. J. Metz, and M. Wolf, “Measuring tissue hemodynamics and oxygenation by continuous-wave functional near-infrared spectroscopy—how robust are the different calculation methods against movement artifacts?,” *Physiol Meas*, vol. 35, no. 4, pp. 717–734, Apr. 2014, doi: 10.1088/0967-3334/35/4/717.

[22] M. Ferrari and V. Quaresima, “A brief review on the history of human functional near-infrared spectroscopy (fNIRS) development and fields of application,” *Neuroimage*, vol. 63, no. 2, pp. 921–935, Nov. 2012, doi: 10.1016/j.neuroimage.2012.03.049.

[23] P. Pinti *et al.*, “The present and future use of functional near-infrared spectroscopy (fNIRS) for cognitive neuroscience,” *Ann N Y Acad Sci*, vol. 1464, no. 1, pp. 5–29, Mar. 2020, doi: 10.1111/nyas.13948.

[24] Md. A. Rahman, A. B. Siddik, T. K. Ghosh, F. Khanam, and M. Ahmad, “A Narrative Review on Clinical Applications of fNIRS,” *J Digit Imaging*, vol. 33, no. 5, pp. 1167–1184, Oct. 2020, doi: 10.1007/s10278-020-00387-1.

[25] F. Zheng, R. Sheinberg, M.-S. Yee, M. Ono, Y. Zheng, and C. W. Hogue, “Cerebral Near-Infrared Spectroscopy Monitoring and Neurologic Outcomes in Adult Cardiac Surgery Patients,” *Anesth Analg*, vol. 116, no. 3, pp. 663–676, Mar. 2013, doi: 10.1213/ANE.0b013e318277a255.

[26] D. W. Green and G. Kunst, “Cerebral oximetry and its role in adult cardiac, non-cardiac surgery and resuscitation from cardiac arrest,” *Anaesthesia*, vol. 72, no. S1, pp. 48–57, Jan. 2017, doi: 10.1111/anae.13740.

[27] S. Purkayastha and F. Sorond, “Transcranial Doppler ultrasound: technique and application,” in *Seminars in neurology*, Thieme Medical Publishers, 2012, pp. 411–420.

[28] C. Lewis, S. D. Parulkar, J. Bebawy, S. Sherwani, and C. W. Hogue, “Cerebral Neuromonitoring During Cardiac Surgery: A Critical Appraisal With an Emphasis on Near-Infrared Spectroscopy,” *J Cardiothorac Vasc Anesth*, vol. 32, no. 5, pp. 2313–2322, Oct. 2018, doi: 10.1053/j.jvca.2018.03.032.

[29] S. Beniczky and D. L. Schomer, “Electroencephalography: basic biophysical and technological aspects important for clinical applications,” *Epileptic Disorders*, vol. 22, no. 6, pp. 697–715, 2020.

[30] P. L. Purdon, A. Sampson, K. J. Pavone, and E. N. Brown, “Clinical Electroencephalography for Anesthesiologists,” *Anesthesiology*, vol. 123, no. 4, pp. 937–960, Oct. 2015, doi: 10.1097/ALN.0000000000000841.

[31] F. W. Sharbrough, “Electrical fields and recording techniques,” *Current practice of clinical electroencephalography*, pp. 29–49, 1990.

[32] Y. Sun, C. Wei, V. Cui, M. Xiu, and A. Wu, “Electroencephalography: Clinical Applications During the Perioperative Period,” *Front Med (Lausanne)*, vol. 7, Jun. 2020, doi: 10.3389/fmed.2020.00251.

[33] S. Finnigan, A. Wong, and S. Read, “Defining abnormal slow EEG activity in acute ischaemic stroke: Delta/alpha ratio as an optimal QEEG index,” *Clinical Neurophysiology*, vol. 127, no. 2, pp. 1452–1459, Feb. 2016, doi: 10.1016/j.clinph.2015.07.014.

[34] A. Alkhachroum *et al.*, “Electroencephalogram in the intensive care unit: a focused look at acute brain injury,” *Intensive Care Med*, vol. 48, no. 10, pp. 1443–1462, Oct. 2022, doi: 10.1007/s00134-022-06854-3.

[35] S. P. Finnigan, M. Walsh, S. E. Rose, and J. B. Chalk, “Quantitative EEG indices of sub-acute ischaemic stroke correlate with clinical outcomes,” *Clinical Neurophysiology*, vol. 118, no. 11, pp. 2525–2532, Nov. 2007, doi: 10.1016/j.clinph.2007.07.021.

[36] H. L. Edmonds, B. L. Ganzel, and E. H. Austin, “Cerebral Oximetry for Cardiac and Vascular Surgery,” *Semin Cardiothorac Vasc Anesth*, vol. 8, no. 2, pp. 147–166, Jun. 2004, doi: 10.1177/108925320400800208.

[37] C. O’Brien, T. W. Okell, M. Chiew, and P. Jezzard, “Volume-localized measurement of oxygen extraction fraction in the brain using MRI,” *Magn Reson Med*, vol. 82, no. 4, pp. 1412–1423, Oct. 2019, doi: 10.1002/mrm.27823.

[38] J. A. H. R. Claassen, D. H. J. Thijssen, R. B. Panerai, and F. M. Faraci, “Regulation of cerebral blood flow in humans: physiology and clinical implications of autoregulation,” *Physiol Rev*, vol. 101, no. 4, pp. 1487–1559, Oct. 2021, doi: 10.1152/physrev.00022.2020.

[39] A. Z. Apaydın, “Antegrade cerebral perfusion: A review of its current application,” *The Turkish Journal of Thoracic and Cardiovascular Surgery*, vol. 29, no. 1, pp. 1–4, Jan. 2021, doi: 10.5606/tgkdc.dergisi.2021.21255.

[40] L. Rivera-Lara *et al.*, “Predictors of outcome with cerebral autoregulation monitoring: a systematic review and meta-analysis,” *Crit Care Med*, vol. 45, no. 4, pp. 695–704, 2017.

[41] M. H. Olsen, C. G. Riberholt, J. Mehlsen, R. M. Berg, and K. Møller, “Reliability and validity of the mean flow index (Mx) for assessing cerebral autoregulation in humans: A systematic review of the methodology,” *Journal of Cerebral Blood Flow & Metabolism*, vol. 42, no. 1, pp. 27–38, Jan. 2022, doi: 10.1177/0271678X211052588.

[42] A. S. S. Meel-van den Abeelen, A. H. E. A. van Beek, C. H. Slump, R. B. Panerai, and J. A. H. R. Claassen, “Transfer function analysis for the assessment of cerebral autoregulation using

spontaneous oscillations in blood pressure and cerebral blood flow," *Med Eng Phys*, vol. 36, no. 5, pp. 563–575, May 2014, doi: 10.1016/j.medengphy.2014.02.001.

[43] A. S. S. Meel-van den Abeelen *et al.*, "Between-centre variability in transfer function analysis, a widely used method for linear quantification of the dynamic pressure–flow relation: The CARNet study," *Med Eng Phys*, vol. 36, no. 5, pp. 620–627, May 2014, doi: 10.1016/j.medengphy.2014.02.002.

[44] A. A. Phillips, F. H. Chan, M. M. Z. Zheng, A. V Krassioukov, and P. N. Ainslie, "Neurovascular coupling in humans: Physiology, methodological advances and clinical implications," *Journal of Cerebral Blood Flow & Metabolism*, vol. 36, no. 4, pp. 647–664, Apr. 2016, doi: 10.1177/0271678X15617954.

[45] C. Iadecola, "The Neurovascular Unit Coming of Age: A Journey through Neurovascular Coupling in Health and Disease," *Neuron*, vol. 96, no. 1, pp. 17–42, Sep. 2017, doi: 10.1016/j.neuron.2017.07.030.

[46] G. J. Del Zoppo, M. Moskowitz, and M. Nedergaard, "The neurovascular unit and responses to ischemia," *Stroke Pathophysiol. Diagnosis, Manag*, 2015.

[47] N. Eleveld, "Manuscript in Press," *Pending*, 2024.

[48] L. Newman, H. Nolan, D. Carey, R. B. Reilly, and R. A. Kenny, "Age and sex differences in frontal lobe cerebral oxygenation in older adults—Normative values using novel, scalable technology: Findings from the Irish Longitudinal Study on Ageing (TILDA)," *Arch Gerontol Geriatr*, vol. 87, p. 103988, Mar. 2020, doi: 10.1016/j.archger.2019.103988.

[49] C. H. Tegeler *et al.*, "Transcranial Doppler velocities in a large, healthy population," *Journal of Neuroimaging*, vol. 23, no. 3, pp. 466–472, 2013.

[50] C. W. Hoedemaekers *et al.*, "Low cerebral blood flow after cardiac arrest is not associated with anaerobic cerebral metabolism," *Resuscitation*, vol. 120, pp. 45–50, Nov. 2017, doi: 10.1016/j.resuscitation.2017.08.218.

[51] A. G. Correa, E. Laciar, H. D. Patiño, and M. E. Valentinuzzi, "Artifact removal from EEG signals using adaptive filters in cascade," in *Journal of Physics: Conference Series*, IOP Publishing, 2007, p. 012081.

[52] R. B. Panerai *et al.*, "Transfer function analysis of dynamic cerebral autoregulation: A CARNet white paper 2022 update," *Journal of Cerebral Blood Flow & Metabolism*, vol. 43, no. 1, pp. 3–25, Jan. 2023, doi: 10.1177/0271678X221119760.

[53] J. A. Claassen, A. S. Meel-van den Abeelen, D. M. Simpson, and R. B. Panerai, "Transfer function analysis of dynamic cerebral autoregulation: A white paper from the International Cerebral Autoregulation Research Network," *Journal of Cerebral Blood Flow & Metabolism*, vol. 36, no. 4, pp. 665–680, Apr. 2016, doi: 10.1177/0271678X15626425.

[54] M. H. Olsen, C. G. Riberholt, R. R. Plovsing, K. Møller, and R. M. G. Berg, "Reliability of the mean flow index (Mx) for assessing cerebral autoregulation in healthy volunteers," *Physiol Rep*, vol. 9, no. 12, Jun. 2021, doi: 10.14814/phy2.14923.

[55] K. Brady *et al.*, "Real-Time Continuous Monitoring of Cerebral Blood Flow Autoregulation Using Near-Infrared Spectroscopy in Patients Undergoing Cardiopulmonary Bypass," *Stroke*, vol. 41, no. 9, pp. 1951–1956, Sep. 2010, doi: 10.1161/STROKEAHA.109.575159.

[56] R. Zhang, J. H. Zuckerman, C. A. Giller, and B. D. Levine, “Transfer function analysis of dynamic cerebral autoregulation in humans,” *American Journal of Physiology-Heart and Circulatory Physiology*, vol. 274, no. 1, pp. H233–H241, 1998.

[57] S. S. Shapiro and M. B. Wilk, “An analysis of variance test for normality (complete samples),” *Biometrika*, vol. 52, no. 3–4, pp. 591–611, Dec. 1965, doi: 10.1093/biomet/52.3-4.591.

[58] E. W. Weisstein, “Bonferroni correction,” *https://mathworld. wolfram. com/*, 2004.

[59] F.-S. F. Yao, C.-C. A. Tseng, C.-Y. A. Ho, S. K. Levin, and P. Illner, “Cerebral oxygen desaturation is associated with early postoperative neuropsychological dysfunction in patients undergoing cardiac surgery,” *J Cardiothorac Vasc Anesth*, vol. 18, no. 5, pp. 552–558, Oct. 2004, doi: 10.1053/j.jvca.2004.07.007.

[60] P. E. Bickler, J. R. Feiner, and M. D. Rollins, “Factors Affecting the Performance of 5 Cerebral Oximeters During Hypoxia in Healthy Volunteers,” *Anesth Analg*, vol. 117, no. 4, pp. 813–823, Oct. 2013, doi: 10.1213/ANE.0b013e318297d763.

[61] J. Zhao *et al.*, “Linking Resting-State Networks in the Prefrontal Cortex to Executive Function: A Functional Near Infrared Spectroscopy Study,” *Front Neurosci*, vol. 10, Oct. 2016, doi: 10.3389/fnins.2016.00452.

[62] A. Casati *et al.*, “Continuous Monitoring of Cerebral Oxygen Saturation in Elderly Patients Undergoing Major Abdominal Surgery Minimizes Brain Exposure to Potential Hypoxia,” *Anesth Analg*, vol. 101, no. 3, pp. 740–747, Sep. 2005, doi: 10.1213/01.ane.0000166974.96219.cd.

[63] A. Deschamps *et al.*, “Cerebral Oximetry Monitoring to Maintain Normal Cerebral Oxygen Saturation during High-risk Cardiac Surgery,” *Anesthesiology*, vol. 124, no. 4, pp. 826–836, Apr. 2016, doi: 10.1097/ALN.0000000000001029.

[64] B. Subramanian *et al.*, “A Multicenter Pilot Study Assessing Regional Cerebral Oxygen Desaturation Frequency During Cardiopulmonary Bypass and Responsiveness to an Intervention Algorithm,” *Anesth Analg*, vol. 122, no. 6, pp. 1786–1793, Jun. 2016, doi: 10.1213/ANE.0000000000001275.

[65] C. V. Ghincea *et al.*, “Utility of neuromonitoring in hypothermic circulatory arrest cases for early detection of stroke: Listening through the noise,” *J Thorac Cardiovasc Surg*, vol. 162, no. 4, pp. 1035-1045.e5, Oct. 2021, doi: 10.1016/j.jtcvs.2020.01.090.

[66] M. B. Skrifvars, M. Sekhon, and E. A. Åneman, “Monitoring and modifying brain oxygenation in patients at risk of hypoxic ischaemic brain injury after cardiac arrest,” *Crit Care*, vol. 25, no. 1, p. 312, Dec. 2021, doi: 10.1186/s13054-021-03678-3.

[67] T. McMorris, B. J. Hale, M. Barwood, J. Costello, and J. Corbett, “Effect of acute hypoxia on cognition: A systematic review and meta-regression analysis,” *Neurosci Biobehav Rev*, vol. 74, pp. 225–232, Mar. 2017, doi: 10.1016/j.neubiorev.2017.01.019.

[68] M. Lacerte, A. Hays Shapshak, and F. B. Mesfin, “Hypoxic Brain Injury,” StatPearls.

[69] M. Holzschuh, C. Woertgen, C. Metz, and A. Brawanski, “Comparison of changes in cerebral blood flow and cerebral oxygen saturation measured by near infrared spectroscopy (NIRS) after acetazolamide,” *Acta Neurochir (Wien)*, vol. 139, no. 1, pp. 58–62, Jan. 1997, doi: 10.1007/BF01850869.

[70] S. Moritz, P. Kasprzak, M. Arlt, K. Taeger, and C. Metz, “Accuracy of Cerebral Monitoring in Detecting Cerebral Ischemia during Carotid Endarterectomy,” *Anesthesiology*, vol. 107, no. 4, pp. 563–569, Oct. 2007, doi: 10.1097/01.anes.0000281894.69422.ff.

[71] P. Schramm *et al.*, “Impaired cerebrovascular autoregulation in patients with severe sepsis and sepsis-associated delirium,” *Crit Care*, vol. 16, pp. 1–8, 2012.

[72] J. Naqvi, K. H. Yap, G. Ahmad, and J. Ghosh, “Transcranial Doppler ultrasound: a review of the physical principles and major applications in critical care,” *Int J Vasc Med*, vol. 2013, 2013.

[73] P. H. Tonner and B. Bein, “Classic electroencephalographic parameters: Median frequency, spectral edge frequency etc,” *Best Pract Res Clin Anaesthesiol*, vol. 20, no. 1, pp. 147–159, Mar. 2006, doi: 10.1016/j.bpa.2005.08.008.

[74] W. M. McDevitt, T. Gul, T. J. Jones, B. R. Scholefield, S. Seri, and N. E. Drury, “Perioperative electroencephalography in cardiac surgery with hypothermic circulatory arrest: a narrative review,” *Interact Cardiovasc Thorac Surg*, vol. 35, no. 4, Sep. 2022, doi: 10.1093/icvts/ivac198.

[75] D. Jiang *et al.*, “Normal variations in brain oxygen extraction fraction are partly attributed to differences in end-tidal CO_2,” *Journal of Cerebral Blood Flow & Metabolism*, vol. 40, no. 7, pp. 1492–1500, Jul. 2020, doi: 10.1177/0271678X19867154.

[76] E. W. Lang, H. M. Mehdorn, N. W. C. Dorsch, and M. Czosnyka, “Continuous monitoring of cerebrovascular autoregulation: a validation study,” *J Neurol Neurosurg Psychiatry*, vol. 72, no. 5, pp. 583–586, 2002.

[77] I. A. Crippa *et al.*, “Impaired cerebral autoregulation is associated with brain dysfunction in patients with sepsis,” *Crit Care*, vol. 22, no. 1, p. 327, Dec. 2018, doi: 10.1186/s13054-018-2258-8.

[78] A. H. E. A. Van Beek, J. A. H. R. Claassen, M. G. M. O. Rikkert, and R. W. M. M. Jansen, “Cerebral autoregulation: an overview of current concepts and methodology with special focus on the elderly,” *Journal of Cerebral Blood Flow & Metabolism*, vol. 28, no. 6, pp. 1071–1085, 2008.

[79] A. N. Naguib *et al.*, “The correlation of two cerebral saturation monitors with jugular bulb oxygen saturation in children undergoing cardiopulmonary bypass for congenital heart surgery,” *J Intensive Care Med*, vol. 32, no. 10, pp. 603–608, 2017.

[80] N. Eleveld *et al.*, “The Influence of Extracerebral Tissue on Continuous Wave Near-Infrared Spectroscopy in Adults: A Systematic Review of In Vivo Studies,” *J Clin Med*, vol. 12, no. 8, p. 2776, Apr. 2023, doi: 10.3390/jcm12082776.

[81] G. S. Fisch, “Visual Inspection of Data Revisited: Do the Eyes Still Have It?,” *Behav Anal*, vol. 21, no. 1, pp. 111–123, Apr. 1998, doi: 10.1007/BF03392786.

8. Appendix

8.1. Boxplots from the transfer function analysis

Figures 18 to 21 show the outcomes of the transfer function analysis for patient 3 in boxplots. For each of the 4 frequency bands, phase, gain, and coherence are analyzed for both hypoxic (n=30) and normoxic (n=5) segments.

Figure 18 shows outcomes in the VLF range. Outcomes in hypoxia show higher variance compared to normoxia.

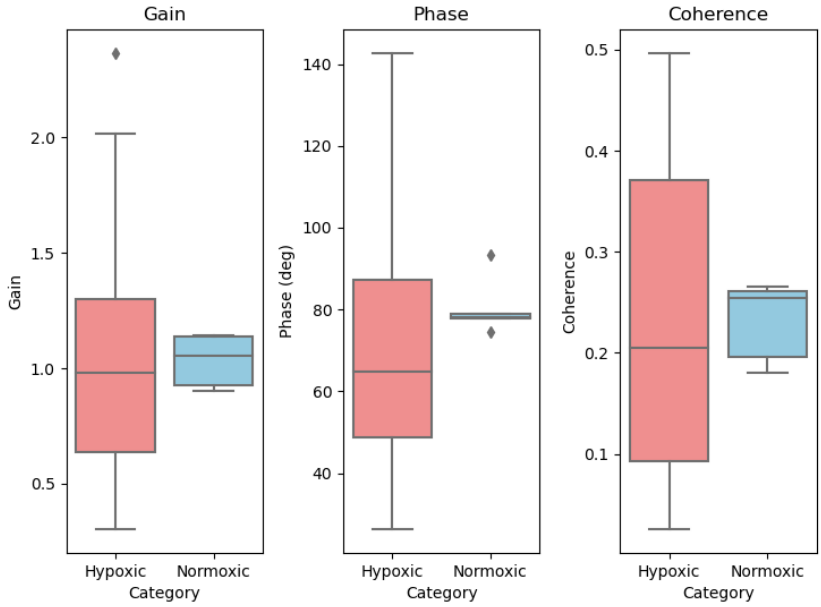

Figure 18: Transfer function analysis (TFA) results for the 0.02-0.07Hz very low frequency (VLF) range.

Figure 19 shows outcomes in the LF range. For hypoxia, median and IQR show higher values for gain and lower values for phase. Coherences distributions appear similar.

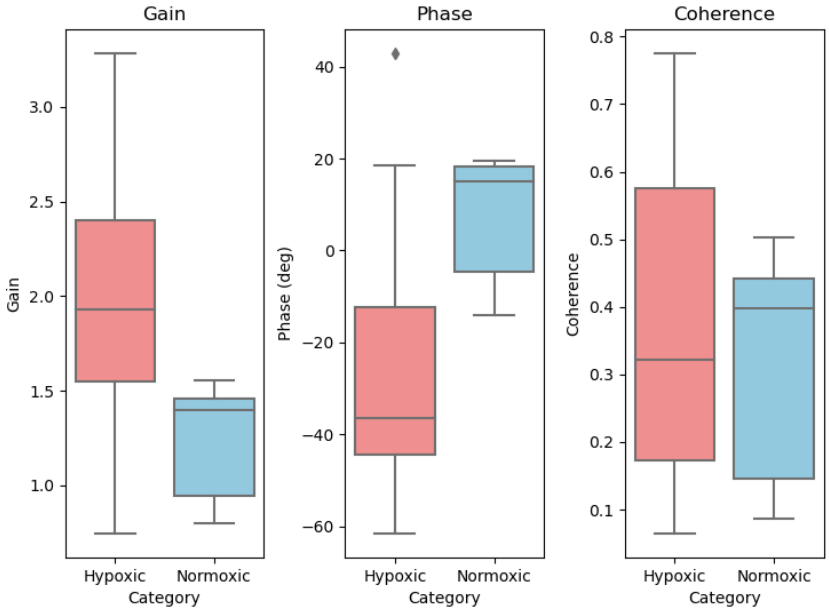

Figure 19: Transfer function analysis (TFA) results for the 0.07-0.20Hz low frequency (LF) range.

Figure 20 shows outcomes in the HF range. For the gain, the median and IQR are similar, but the hypoxic dataset shows some low gain values <1.0. The phase of hypoxic and normoxic segments are both very close 0.0. Coherence distributions are overlapping, but the variance appear greater in hypoxia.

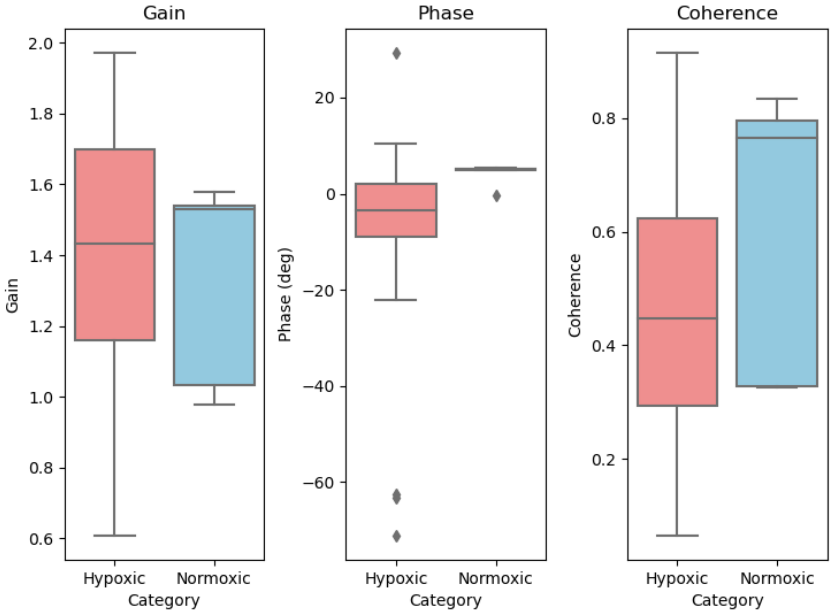

Figure 20: Transfer function analysis (TFA) results for the 0.20-0.50Hz high frequency (HF) range.

Figure 21 shows outcomes in the total frequency range. Hypoxia shows a higher gain and lower phase, close to 0.0. Coherence distributions are overlapping, but the variance appear greater in hypoxia.

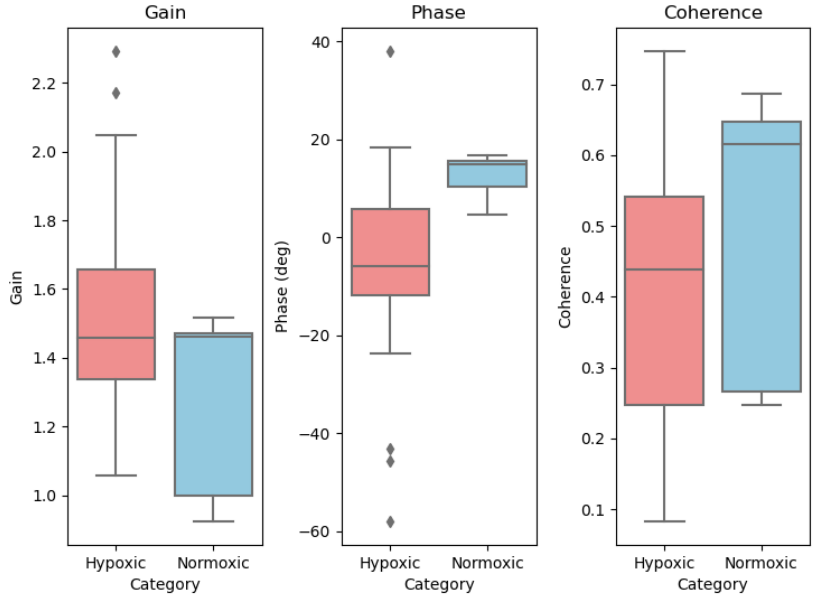

Figure 21: Transfer function analysis (TFA) results for the total 0.02-0.50Hz frequency range